Martian Gully Activity and the Gully Sediment Transport System

Colin Dundas, Susan Conway, Glen Cushing

Martian Gully Activity and the Gully Sediment Transport System

Colin M. Dundas[a] *

Susan J. Conway[b]

Glen E. Cushing[a]

[a]U.S. Geological Survey, Astrogeology Science Center, 2255 N. Gemini Dr., Flagstaff, AZ 86001, USA (cdundas@usgs.gov).

[b]Nantes Université – Université d'Angers – Le Mans Université, CNRS UMR 6112 Laboratoire de Planétologie et Géodynamique, 2 rue de la Houssinière, 44322 Nantes France.

*Corresponding author.

Abstract

The formation process for Martian gullies is a critical unknown for understanding recent climate conditions. Leading hypotheses include formation by snowmelt in a past climate, or formation via currently active CO_2 frost processes. This paper presents an expanded catalog of more than 300 recent flows in gullies. The results indicate that sediment transport in current gully flows moves the full range of materials needed for gully formation. New flows are more likely to transport boulders in gullies that have pre-existing boulder-covered aprons, indicating that current flows are transporting the same materials required for gully formation overall. The distribution of gully activity frequencies can be described by a power law and indicates that the recurrence intervals for flows in individual gullies are commonly tens to hundreds of Mars years. Over the last ~300 kyr, climate variations have been modest but individual gullies have had tens to thousands of flow events. This could be sufficient to account for the entirety of gully formation in some cases, although the same processes are likely to have occurred further in the past. For any gullies that may have initiated under higher-obliquity conditions, this level of recent activity indicates that the observable morphology has been shaped by CO_2-driven flows. These observations of sediment transport and the tempo of gully activity are consistent with gully formation entirely by CO_2 frost processes, likely with spatial and temporal variability, but with no role required for liquid water.

1. Introduction

The discovery of new flows associated with Martian gullies (Malin et al., 2006) and subsequent observation of widespread activity (e.g., Dundas et al., 2019a) have opened an important debate in gully studies. The marked seasonality of present-day flows (e.g., Harrison et al., 2009; Dundas et al., 2010; 2012) indicates that seasonal CO_2 frost is the cause of current activity. However, it is debated whether such activity is the sole cause of gully formation (e.g., Hoffman, 2002; Pilorget and Forget, 2016; Dundas et al., 2019a) or whether other processes involving liquid water may have also contributed in the past (e.g., Malin and Edgett, 2000; Costard et al., 2002; Christensen, 2003; Conway et al., 2019). The distinction is of key importance for studies of recent Martian climate, surface evolution, and habitability, because CO_2 frost-driven formation would indicate a generally dry Late Amazonian climate, but formation via melting and runoff would recurring liquid water.

Multiple CO_2 frost-based processes have been proposed for gullies. Hoffman (2002) proposed gas-lubricated flow initiated by basal sublimation, Ishii and Sasaki (2004) suggested avalanching frost, and Pilorget and Forget (2016) further developed the basal-sublimation-triggering model. Dundas et al. (2019a) found that defrosting spots expected for basal sublimation were rare in gullies below 40º latitude. Dundas et al. (2019a) and de Haas et al. (2019b) therefore further developed the gas-lubricated flow model, demonstrating that energy dissipation during a flow with incorporated CO_2 frost would generate substantial vapor within the flow and allow it to behave similarly to an aqueous debris flow on Earth.

57 It is difficult to rule out the possibility of past liquid water based on orbital remote
58 sensing. However, the CO_2 model can be tested by investigating whether observed CO_2
59 processes are sufficient to create gullies; if this is the case, then there is no need to invoke
60 additional past processes. One key test is whether the current flows erode and transport
61 the material required to create the observed landforms.
62 Many gullies form within mid-latitude mantle deposits, which can thickly bury
63 pole-facing slopes (e.g., Christensen, 2003; Aston et al., 2011; Conway and Balme, 2014;
64 Dickson et al., 2015). Although generally considered to be a deposit of ice and dust (e.g.,
65 Mustard et al., 2001), the mantle deposits on slopes often contain boulders. However,
66 alcove volumes exceed apron volumes in many cases, indicating a significant ice content
67 (up to 95% by volume) in the mantle (Conway and Balme, 2014; Gulick et al., 2019).
68 Some alcoves are the result of simply removing this mantle, with minimal erosion of the
69 underlying slope; other alcoves substantially erode into bedrock (e.g., Aston et al., 2011;
70 de Haas et al., 2015b). De Haas et al. (2015b) also found that among gullies with alcoves
71 eroded into bedrock, cross-sectional exposures of the apron usually revealed isolated
72 boulders or boulder lenses within a finer-grained matrix, which they interpreted as
73 evidence of debris flows. Within aprons of gullies eroded only into the latitude-dependent
74 mantle, boulders were rare.
75 If gullies are actively forming today, similar relationships should exist between
76 the eroded material in the alcoves and that transported by the flows. In other words, in
77 gullies that require erosion and transport of rocky material, the current flows should be
78 capable of transporting that rocky material. Alternatively, present-day flows could be

relatively incapable of transport, requiring more vigorous flows and possibly different processes in the past. This relationship is investigated below.

2. Data and Methods

2.1. Change Detection Survey

The initial stage of this investigation was compilation of an updated gully change detection survey. The primary data set is images from the High Resolution Imaging Science Experiment (HiRISE; McEwen et al., 2007) on board the Mars Reconnaissance Orbiter (MRO; Zurek and Smrekar, 2007). HiRISE images are typically 5-6 km wide and 10-20 km long and include a central color swath acquired through near-infrared and blue-green filters in addition to the broad red channel. The Reduced Data Records (RDRs) are map-projected and normally have a scale of 25 or 50 cm/pixel. The MRO orbit is designed so that the local time in images is always near 3 PM, although the incidence angle and sub-solar azimuth vary seasonally. This survey makes use of data acquired through MRO orbit 61,299 (August 24, 2020), which corresponds to approximately L_S=70° of Mars Year (MY) 35 in the calendar enumerated by Clancy et al. (2000) and Piqueux et al. (2015). HiRISE began transition phase imaging at L_S=114° of MY 28. Earlier versions of this survey used data through MRO orbit 25,000 (Dundas et al., 2012), 35,599 (Dundas et al., 2015b) and 48,999 (Dundas et al., 2019a), corresponding to MY31 L_S=35°, MY32 L_S=96°, and MY33 L_S=295° respectively. Both the number of monitoring sites and the time baseline at many of the sites have expanded between each iteration. Monitoring sites used for this project are those with repeat HiRISE coverage of non-dune gullies with the first and last images separated by at least 4000 MRO orbits

(approximately 10 months). This survey covers 513 sites in the southern hemisphere and 189 in the north, where a site is defined as a series of overlapping HiRISE images; a large crater or other feature may include multiple sites, sometimes adjacent. Table S1 summarizes the monitoring sites, including information about the time baseline and quality of the matching images, and Figure 1 shows their geographic distribution. Figure 2 shows an example of a change that carved new gully channel segments and re-incised old channel reaches.

In order to estimate the frequency of flows on a per-gully basis, the number of gullies at one hundred southern-hemisphere sites were counted and divided into two categories: well-developed gullies with substantial widening and deepening of alcoves, and poorly developed gullies with small or absent alcoves. This approach was only applied to a subset of monitoring sites because a single gully is often not a well-defined feature: alcoves and channels merge, branch, and subdivide. Due to this inherent uncertainty there is little value to attempting a precise accounting for all sites. These data are used for two purposes: first, comparing the characteristics of early and later monitoring sites to understand data biases, and second, derivation of an approximate per-gully flow recurrence interval.

Since December 2016, the HiRISE team has made an effort to more frequently acquire change-detection images that closely match the viewing and lighting angles of older observations. A close match in these parameters leads to easier comparisons and more effective change detection. These observations (informally referred to as "HiKERs", for HiRISE checK for Exact Repeats, the method used to find opportunities to acquire such images) are specifically designed to have a convergence angle between

the two images (viewing angle difference) of <5° and to match the incidence angle and sub-solar azimuth to within 5° and 7°, respectively. Lower-quality matches are still acquired and used in this study, but the effort to collect HiKER observations has resulted in more high-quality comparison images in recent years.

The gully change survey in this work generally uses the same methods as Dundas et al. (2015b; 2019a) which are briefly summarized here. Sections of the RDR images were extracted at 1 m/pixel, locally aligned (translations only, shifting as needed for each local comparison), and blink-compared to look for changes. Since the RDRs are not orthorectified to a high-resolution Digital Terrain Model (DTM) there is typically some distortion, but this was considered an acceptable compromise since orthoimage coverage is limited to a small fraction of the total number of sites. The search was focused on the areas of the channel terminus and apron, and in most cases only examined alcoves and upper channels to the extent that they fell within the same swaths of the image. Images spanning the entire timeframe of HiRISE observations of each site through orbit 61,299 were compared, often with multiple comparisons made per site depending on the quality of match of the illumination and geometry. In rare instances the earliest or latest image was not used, if it was a low-quality comparison and represented only a short additional time increment. Changes in gullies were recorded and documented in Table S2. Table S2 also includes non-gully flow events that are very close to gullies and may represent early stages of new gully formation. Unlike previous work, this tabulation only includes changes that have HiRISE coverage from before the flow and give frequencies based only on such events; this excludes only 11 events and provides a much more controlled and uniform quality of coverage over each study site. Information recorded in Table S2

includes the monitoring site, the location of the change in a reference HiRISE image, the time constraints on the change, and information about the observed changes to albedo and topography. The latter includes whether the flow was bright or dark relative to the surroundings, its color in HiRISE images, whether topographic changes were observed, and whether channel incision was detected. HiRISE relative color uses the color RDR images, which have the HiRISE near-infrared channel assigned to display red, the HiRISE red channel assigned to green, and the HiRISE blue-green channel assigned to blue, and the color images are stretched to enhance contrast. This does not approximate true color but maximizes the color-contrast information available from HiRISE. Nearly all flows with distinctive color appear blue or yellow in this color scheme; "blue" flows are those that are particularly reflective in the HiRISE blue-green channel relative to the surrounding surface, and "yellow" flows are particularly reflective in the red and near-infrared channels.

Flows were classified as "major flows" if they substantially altered the channel morphology, "flows" if they had minor observable topographic changes, and "thin flows" if they had no discernable topographic effect. Detection of topographic changes depends on the image lighting and the quality of the match between before-and-after images, so the tabulated changes should be considered a lower bound. "Channel incision" refers to any removal of material within a channel, ranging from new channel reaches or clearing of infilled channels to small-scale widening or removal of within-channel deposits.

Table S2 also includes information about the gully substrate. This was subdivided into categories: the primary material removed to create the alcove, the material into which the channel is incised, the apron deposits, and the nature of the material deposited

by the new flow. Alcove material was categorized as rock, mantle (thick deposits mantling the slope, which may include a substantial component of rocks but are distinct from in-place outcrops), mixed (alcoves incising both rock outcrops and other materials, including those where both mantle deposits and underlying rocky material were eroded), sand, or other (few or no boulders resolved by HiRISE). The incised material, apron, and new deposit were categorized as mixed (many boulders among finer sediment), sand, or other. Sand was characterized by rippled texture and usually has a dark tone relative to the surroundings; new deposits of sand may lack ripples but can be characterized as such if the incised material is sandy. Sand was classified conservatively and some material classified as "other" is likely sand that does not definitively show these characteristics. "Other" material could also be dust or other sediments with grain sizes that are not resolvable by HiRISE. Gradations exist both along any individual gully system, and between materials with various levels of rockiness, but this enables a first-order classification of what is eroded, transported, and deposited to create gullies. De Haas et al. (2015b) looked at cross-sectional exposures of gully deposits in channels and noted that the surface morphology may be reworked; here we are interested in the presence of boulders, which are not likely to be removed by modification processes on the timescale of recent flow events.

Table S2 includes some examples of changes in gullies that did not indicate flow through the gully system, such as shifting rocks. The same information is tabulated for each of these changes. Recurring Slope Lineae (McEwen et al., 2011) and albedo changes attributed to aeolian processes were not recorded but occur in and around many gullies. Small defrosting spots and flows (e.g., Hansen et al., 2011) were also excluded as in

Dundas et al. (2015b), although large flows burying frost are included. The two appear to be distinct: in addition to size differences, the small defrosting flows (dubbed "flow-like streaks" by Raack et al. (2020)) grow incrementally for many weeks.

The list of flow events through the gully system in Table S2 is as complete as possible given the limitations of the survey methods noted above. Nevertheless, this data set is certainly incomplete and should be regarded as a lower bound on the flow activity across the sites and time intervals covered by HiRISE. Only changes considered definite are included here; possible or probable candidates were excluded. This standard inevitably excludes some real flows, particularly those that are small or subtle, or that are only covered by data that has a poor match in lighting or viewing angles or by poor quality data. Newer observations have allowed detection or confirmation of some changes that were present in older data but which were missed or considered unconfirmed for these reasons. Thin flows might form and fade entirely in a long interval between HiRISE observations, especially if the interval includes a major dust storm; planet-encircling dust events occurred in MY 29 and MY 35. Some gully flows are visible only while shadowed (Dundas et al., 2012; 2015b); these are likely thin flows that are visible only when contrasted against underlying frost. Others are obvious when covering frost but marginally detectable in defrosted images (Fig. 3). Comparisons generally used well-illuminated data when available and shadows were not systematically searched for more such flows, they are tabulated here when known but likely undercounted. Additionally, our search focused on the apron and channel terminus region since we are interested in flows that traversed most of the gully system, so changes that were restricted to the alcove or upper channel are likely to be missed. However, once

flows were detected their entire extent was examined, and nearly all initiated in the alcove.

The non-flow changes in gullies reported in Table S2 are highly incomplete, both because searching for such (often smaller) changes was not the focus of this work and because they are inherently more difficult to observe. Many are in alcoves, which can have complicated shadows and often were not searched completely. They are provided as examples of non-flow processes and their role in gully modification is discussed below, but no attempt was made to find and catalog every such change. Other examples of non-flow changes in gullies include rockfalls observed in Gasa crater (Harrison et al., 2015) and changing bright patches attributed to exposure and sublimation of ice (Dundas et al., 2019a; Khuller and Christensen, 2021).

A site in Hale crater (35.2 °S, 324.7 °E; all coordinates herein use planetocentric latitude and east longitude) examined in detail by de Haas et al. (2019b) provides information on completeness. This survey documented six flow events at this site, while they reported over fifty changes. This large discrepancy has several causes. De Haas et al. (2019b) examined orthorectified HiRISE images, while we used HiRISE RDRs at reduced resolution; small and localized changes are far easier to find with the orthoimages. Six flows were detected in common with de Haas et al. (2019b); a further six had subtle topographic effects that were difficult to discern at 1 m/pix, and four were in small features that were not obvious as gullies at reduced resolution. Four flows had significant topographic changes that terminated in the alcove or upper channel. The remaining 34 were either predominantly albedo changes lacking a well-defined flow shape, or sidewall slumping or minor mass wasting that did not significantly propagate

down the channel. Thus (i) our survey was effective at finding the most significant flows that descended most or all of the channel system, (ii) more flows exist near or below the detection limits of our survey, (iii) more flows exist that only move material in alcoves and upper channels, and (iv) there is common small-scale mass wasting and albedo change in alcoves and channel sidewalls not captured by our survey. Of these, (ii) is an obvious consequence of using non-orthorectified images and reduced resolution, and (iv) describes changes not included in our survey by design; there is too much of such activity to manually document across hundreds of sites and it is often difficult to confirm such changes when images are not an ideal match. The largest concern is issue (iii), but this Hale crater site is a worst-case scenario for detecting such flows: many of the gullies are kilometers long, so large swaths of the upper reaches were not examined even incidentally. However, this comparison serves to emphasize that the detections of gully activity presented here are a lower limit on the total number of gully flows that have occurred with HiRISE coverage. Table S2 only includes the six flows that were observed independently.

To first order the geographic distribution of monitoring sites resembles the overall distribution of gullies (e.g., Harrison et al., 2015). Potential data biases are similar to those in Dundas et al. (2015b). HiRISE targeting is inherently biased towards locations thought to be of interest at HiRISE scale, and fresh-appearing gullies are more likely to be active than those with degraded morphologies (Dundas et al., 2015b). This likely results in over-representation of gullies that appear particularly fresh, and/or which have many gullies. Additionally, sites that are known to be active are subsequently monitored more frequently, although for flows that are not rapidly obscured, frequent monitoring

improves the time constraints but not the detection of changes. Smaller flows are more easily missed and benefit more from well-matched images, which are more likely to exist at sites with many images. These biases are unavoidable when using HiRISE data and are a consequence of the very limited areal coverage. The effect is difficult to quantify, but while it may lead to some over-representation of active gullies in the HiRISE data set the effect is likely not severe. Harrison et al. (2015) identified 4,861 gullied landforms (such as individual craters and massifs) in a near-global survey, while this survey includes >700 monitoring sites; although there is not a perfect one-to-one correspondence between a HiRISE monitoring site and a gullied landform, this does suggest that >10% of gully locations are being sampled, so even in the implausible scenario where no un-monitored sites are active, activity rates are accurate to within one order of magnitude. Numerous factors affect HiRISE target selection, such as the availability of imaging opportunities and competition with other high-priority targets; this can result in biases unrelated to gully properties but forces some randomization of gully targets rather than exclusive imaging of the largest and freshest examples. An initial effort to assess potential bias is provided below by comparing early monitoring sites with more recent additions which are likely to be less eye-catching and thus potentially less active.

3. Results

3.1. Gully activity frequency

As in previous iterations, the broad geographic distribution of monitoring sites (Fig. 1) resembles the overall gully population observed by comprehensive surveys (e.g., Harrison et al., 2015). In the southern hemisphere, 22% of survey sites have documented

flow events with before-and-after HiRISE coverage, while only 8% of sites in the north have such activity. We identified 303 individual flows (of all size classes) and 24 other events in southern-hemisphere gullies; in the north, there are 48 flows and 4 other events. (As noted above, the "other events" tabulation is certainly a substantial under-count.) With increased coverage, some possible spatial trends in activity have emerged. In the south, the most notable feature is a lack of observed activity in gullies in the Dao Vallis region east of the Hellas basin, although this may partly reflect biases in HiRISE targeting. In the north, no activity has been observed equatorward of ~48 °N, and there is a possible concentration of active sites northwest of the Utopia basin.

The number of winter solstices (L_S=90° for the southern hemisphere and 270° for the north) encompassed by the HiRISE monitoring series is used to assess the time duration of observation. This gives an approximate measure of the number of frosted seasons observed, a useful metric since present-day activity is mostly driven by seasonal frost. On average, monitoring series span 3.7 winter solstices in the southern hemisphere and 3.9 in the north. Counting only the years with excellent or good quality comparison data, those averages are 3.0 and 3.6, respectively. To first order these suggest typical per-site event intervals of $(1/0.22)\times 3.0 \cong 14$ Mars years in the southern hemisphere and $(1/0.08)\times 3.6 = 45$ Mars years in the north. These rates treat a site as active or not with no consideration of the number of observed flows.

As noted above, there are both likely biases in the data, and site to site variations in the number, nature, and substrate of gullies. The following section provides several analyses to better understand these activity rates and their uncertainties. This further analysis focuses on the southern hemisphere, because northern flow events are less

309 abundant and over half of the documented examples occur at just two sites, one of which
310 has minimally developed gullies; northern-hemisphere calculations thus suffer more from
311 small-number statistics.

312 In the south, 19% of sites have only poor-quality coverage where change
313 detection is expected to be very difficult. While they are included in the calculation of
314 rates above, the effective fraction of active sites may be ~25% higher and the recurrence
315 interval correspondingly shorter.

316 Figure 4 shows the fraction of sites that have been active as a function of the
317 number of frosted seasons. Unsurprisingly, longer observing baselines correlate with a
318 greater fraction of active sites. (This is not the case in the north (Fig. S1) but the total
319 number of active sites is low.) The figure also shows two curves based on calculated
320 probabilities of activity, for reference: the solid curve shows the probability that a site has
321 been active at least once after N winters, $P(N)$, assuming an annual probability of activity
322 of 0.08. The dashed curve shows $P(N)$ assuming that the probability is 0.05 each year. As
323 discussed below, the annual probability of a flow event varies significantly from site to
324 site, so there is little value to a more precise fit.

325 To derive some estimate of the potential bias from preferentially targeting
326 locations with many fresh-appearing gullies, we compared activity rates for the first 262
327 sites in the southern hemisphere (those analyzed by Dundas et al. (2015b); unlike the
328 main analysis therein, we include gullies on sandy crater-wall slopes here, which adds
329 four additional sites) to those added subsequently. The latter group includes 251 sites and
330 should have much reduced bias from targeting of distinctly fresh or interesting gullies.
331 32% of the sites in the former group have now shown activity with before-and-after

HiRISE coverage, while only 11% of the latter have observed flow changes. The full data set and the late group active frequencies agree well for up to three Mars years before diverging; this may reflect the fact that the earlier sites have been imaged more frequently, while the later sites may have the same time baseline but fewer images. The early-group sites have an average of 1.9 winter solstices of excellent comparison coverage and 1.5 of good quality. The later sites have averages of 1.1 and 1.7 winter solstices, respectively. The difference may also be partially accounted for by a smaller number of gullies per site in the latter group; the earlier sites averaged 9.3 large gullies and 15 small gullies, while the later sites averaged 5.5 and 14. Two significant figures are given in these values for relative comparison, but the ill-defined nature of an individual gully means that those numbers are not as accurate as they appear.

Activity rates clearly vary by site, and there is no one gully activity rate that is valid for the whole population. Figure 5 shows the number of monitoring sites with observed flow rates (flows per site per winter solstice spanned by the data) at or exceeding a range of rates, for the full data set. The same information is shown for the northern hemisphere in Fig. S2. Analysis of these results is pursued further in section 4.

Overall, this analysis suggests that a typical site in the southern hemisphere is likely to have a flow event every ten to twenty Mars years, and a site in the north every fifty Mars years. Individual gullies commonly have flow recurrence intervals ranging from a few to a thousand Mars years. If the Hale crater comparison above is typical, these recurrence intervals may be a factor of several too long for all flows, particularly when flows that are unresolved in our survey and those restricted to the upper reaches are considered. However, the Hale comparison is likely to overcorrect for missed flows at

most sites because the large size of many gullies at the Hale crater site meant that changes restricted to the upper part of the gullies were easily missed. There is little value to better refining these values as a population average because there is also substantial site-to-site variability which is not normally distributed (Fig. 5), so a mean rate is insufficient to fully describe the population. More useful next steps would improve understanding of (i) individual sites, and (ii) the distribution of activity rates across the full population.

3.2. Highly active sites

There is a wide range of variability in activity rates, and no obvious physical property that distinguishes highly active from less active sites. This section provides a brief description of each location that has four or more documented flows. In the south there are many such sites:

- Jintur crater (50 °S, 294.6 °E; 18 flows; coordinates are for centroid of HiRISE monitoring images, not crater center): Gullies entirely within sand covering the crater wall.
- Gasa crater (35.7 °S, 129.4 °E; 16 flows): very young crater (~1.25 Ma; Schon et al., 2009) with large gully alcoves in bedrock, on the floor of a larger crater that was likely glaciated at the time of the smaller crater's formation (Schon and Head, 2012). Diverse activity includes many flows including major flows altering gully morphology, with channel incision and boulder transport, as well as minor flows.

- Sandy massif slope with dunes (40.5 °S, 309.9 °E; 12 flows): Alcove materials are diverse, but most flows involve sandy material including channel formation and erasure.
- Palikir crater (41.4 °S, 202.1 °E; 10 flows in two adjacent sites): well-developed gullies with diverse substrates and flow materials ranging from sand to rocky.
- Dunkassa crater (37.5 °S, 223 °E; 10 flows): Gullies mostly cut into mantling material which is rocky in places, but reaching and eroding bedrock in some cases. Multiple flows with significant topographic effects, including one gully with major flow events in three winters that have resulted in a channel breakout and multi-stage incision of a 50-m-long new channel mouth (Dundas, 2021).
- Selevac crater (37.4 °S, 229 °E; 10 flows in two adjacent sites): Fresh crater hosting numerous gullies with shallow alcoves cut into bedrock. Flows range from thin to major including some that result in visibly thick rocky deposits. The site is notable for having multiple observations of well-defined flows superposing frost, typically showing point sources for flow initiation.
- Avire crater (40.8 °S, 200.3 °E; 9 flows): Gullies mostly in sand covering crater walls, but alcoves often erode some rock. Flows mostly occur within the sand and commonly erode and reshape channels.
- Ariadnes Colles (34.3 °S, 172.3 °E; 10 flows): gullies in mantle material draping the edge of a bedrock mesa (Fig. 6). All events are thin flows visible only in shadow, likely due to contrast with thin coating of frost; there is no visible effect once illuminated, but flow patterns change from year to year.

- Gorgonum Chaos (37.2 °S, 188.3 °E; numerous flows): thin flows in small gullies, which are only visible in shadow similar to the Ariadnes Colles site noted above. Not counted due to the difficulty in accurately counting such small flows in shadow; this site was excluded from the analysis in Fig. 5.
- Sisyphi Cavi (68.5 °S, 1.3 °E; 8 flows): upper alcoves rocky but lower slopes are mantled or covered with smooth deposits. Multiple major flows (cf. Raack et al., 2015; 2020) reshaping channels, occurring in the late stages of seasonal defrosting. The site also has numerous smaller defrosting flows each year, some of which travel down gully channels and thus contribute to the gully sediment flux (Dundas et al., 2012).
- Bari and Arvi craters (39.4 °S, 202.7 °E; 7 flows): Alcoves erode mix of mantle and bedrock. Flows and eroded material mostly have minor topographic effects and often involve sand.
- Satkania crater (32.4 °S, 338.2 °E; 7 flows): Gullies mostly in smooth mantling material but upper alcoves erode rock in some cases. Flows are superficial with little or no resolved topographic effect, and yellow in relative color.
- Langtang crater (38.1 °S, 224.1 °E; 7 flows in two adjacent sites): large gullies, with alcoves mostly in mantle but reaching bedrock in places. Diverse changes including multiple major flows in one gully.
- Galap crater (37.7 °S, 192.9 °E; 6 flows): Fresh crater with gullies cut into bedrock, with substantial boulder transport. One gully has had two major flows.
- Teknaf crater (36 °S, 214.3 °E; 6 flows): Gullies mostly incised into mantle, but alcoves often reach and sometimes cut into the rocky underlying crater wall.

Alcoves have time-variable bright exposures similar to those described by Khuller and Christensen (2021). Flows characteristically bright and yellow. One gully has had three separate flow events including progressive channel extension and incision (Fig. 7).

- Moni crater (47 °S, 18.8 °E; 6 flows): Mostly flows in channels in sand coating crater walls, but also includes other activity. Crater is near the Kaiser crater dune field and sand movement is common.
- Gebog crater (37.3 °S, 124.2 °E; 6 flows): Alcoves remove mantle material and have exposed but not eroded the underlying rocky crater wall. Current activity mostly transports sand within the alcoves.
- Luwuk crater (38.2 °S, 183.9 °E; 6 flows): Alcoves mostly within mantle material but rock has also been eroded. Most current activity involves sand but transport of boulders and non-sand material is also observed.
- Eastern Hale crater (35.1 °S, 324.7 °E; 6 flows documented here, but see above for comparison with de Haas et al. (2019b)): Gullies in mantle deposits and rock on the wall of a large crater. Flows resulted in major morphologic changes including channel extension and terrace formation.
- Northwest Hale crater (34.8 °S, 322.5 °E; 5 flows): Alcoves eroded in a mix of mantle and bedrock. Flows range from superficial albedo features to major topographic changes.
- Corozal crater (38.8 °S, 159.5 °E; 5 flows): Alcoves cut into mix of bedrock and mantle, with fine-grained deposits that have sand or dust bedforms. Flows are

444 dark and sometimes form a halo around the channel; topographic effects are
445 small but channel erosion is observed (e.g., Dundas et al., 2010).
446 • Poso crater (41.1 °S, 201.5 °E; 5 flows): Diverse materials have been eroded in
447 alcoves, but current flows mostly in sand now covering the slope.
448 • Daiyang crater (38.9 °S, 223.7 °E; 5 flows): Alcoves cut into mantle-draped
449 bedrock. Flows result in mostly minor topographic changes, but include channel
450 extension.
451 • Northwest Asimov crater (46.9 °S, 4.3 °E; 5 flows): Superficial flows (both
452 bright and dark) with little or no resolvable topographic effect in channel systems
453 with poorly developed alcoves.
454 • Sisyphi Cavi (71 °S, 1.3 °E; 5 flows): Gullies mostly in smooth mantling material
455 but upper alcoves are rock. Minor topographic changes, including one gully with
456 three separate flow events.
457 • Zhufan crater (37.6 °S, 351.8 °E; 4 flows): Gullies mostly erode mantle deposits
458 but alcoves are also cut into bedrock. Flows exhibit major topographic changes
459 (Fig. 8).
460 • Wukan crater (46.2 °S, 18.7 °E; 4 flows): Mixed alcove materials including
461 poorly developed gullies. Current flows erode and deposit sand.
462
463 In the northern hemisphere the majority of documented flows have occurred
464 within just two craters, which are extreme outliers in their overall activity:
465 • Catota crater (51.7 °S, 333 °E; 19 flows): Extremely fresh crater with very rocky
466 slopes. Gullies are very poorly developed and the tabulation includes flows that

are near but not within the gullies, as this may represent a very early stage of gully formation. Numerous minor topographic changes observed.

- Maur crater (54.5 °N, 305.9 °E; 9 flows): Fresh crater with rocky slopes, and most alcoves are cut into the rock and not very well-developed. Flows have caused major topographic changes. There are several instances where flows descended rocky gullies and then crossed into sandy material and scoured large troughs (Fig. 9); rocks were transported through the sand to the terminus.

There is no clear unifying trend among these sites. They include nearly the full range of substrates, gully morphologies, latitudes, and flow types. Some sites have numerous thin flows with no observable morphologic effect, but this list also includes most of the sites with the most dramatic morphologic changes—there is no obvious trade-off between flow size and frequency. Observations of dune gullies suggest that sandy substrates are particularly active (e.g., Reiss et al., 2010; Diniega et al., 2010; Dundas et al., 2012; 2019a; Pasquon et al., 2016; 2019ab), but this is clearly not the only control, as some of the most active sites are not sandy. Several of the craters hosting gullies are notably fresh and steep, which could contribute to instability and rapid evolution (de Haas et al., 2019a), but others are substantially mantled and not notably fresh.

3.3. Properties of flows

Gully flows are diverse: they can be brighter or darker than the surroundings, and have a wide range of morphologies, from thin flows with no perceptible effect to major events that reshape the gully system. Roughly half of flows are approximately neutral in

albedo; 20% are visibly brighter than the surroundings, and 28% are darker. The proportions of colors where HiRISE color coverage exists are similar: 16% are relatively yellow and 31% are blue. Flow color and relative brightness are strongly correlated: when they have a distinct color, yellow flows are almost always brighter than the surroundings and blue flows almost always darker. There is a hint of spatial variation in relative color (Fig. S3) which is more pronounced in relative brightness (Fig. S4): yellow/bright flows are particularly common northeast of the Argyre basin, and blue/dark flows are more common at higher latitude. Across all HiRISE observations, yellow relative color generally indicates dustier or finer-grained material, and blue indicates sandy or rocky material (Delamere et al., 2010), so these colors could indicate sorting of fine material to the surface of a flow, possibly by escaping gas, or preferential mobilization of fine material in some flows. However, as these are relative colors, the importance of such effects is uncertain.

Flow morphology shows little convincing evidence of geographic variation: major changes and minor or thin flows are both widely distributed (Fig. S5). There are hints of a tendency for thin flows to concentrate in certain regions, such as near 170 °E in the southern hemisphere, but they are weak. Major flows constitute 13% of the data set, flows with minor topographic effects are 67%, and 20% have no visible topographic expression in available HiRISE data. The small fraction of the latter is probably because many more small, subtle flows exist but were not observable within our survey limitations. Nearly half of observed flows (48%) involve some erosion in the channel, ranging from removing small lumps of within-channel material to new breakout channels or extension of channel mouths (Figs. 2, 7). Deposition at channel mouths was not

tracked but also occurred regularly. Most observed flows (70%) reach to or beyond the channel mouth, although the true fraction must be lower due to cases like the Hale crater examples documented by de Haas et al. (2019b). Among the remainder, the morphological effects were often characterized as distributed changes in the channel, with minor erosion and deposition at various places along the channel length. There is rarely a single, straightforward transition from erosion to deposition.

Major flows preferentially occur in larger gullies. Gullies were categorized as well-developed if the alcove was substantially wider and deeper than the lower channel. A majority (63%) of major flows occurred in such gullies, compared with 45% of flows with minor topographic effects and 29% of thin flows. Major flows were almost certain to reach the channel terminus (91%), compared with 60% of flows with minor changes and 79% of thin flows. The high fraction of the latter may be an observational bias: flows with negligible topographic effects are particularly hard to detect with confidence if they do not reach the end of the channel. This is particularly true of the subset of thin flows that are only detectable while in shadow.

3.4. Gully sediment transport

Boulder transport in gullies is not a rare event, as 21% of all documented flows transport boulders. This occurs in 61% of major flows, 20% of flows with minor topographic effects, and 0% of thin flows (by definition). Boulder transport is more likely in gullies where the preexisting apron is boulder-rich. Such aprons are only present for 21% of observed flows, but 43% of flows onto such aprons transported boulders, compared with 15% of flows onto aprons with few or no boulders. Similarly, boulder

536 transport occurs in 40% of flows descending from alcoves with rock outcrop, 17% of
537 those from outcrop/mantle mixtures, and 10% of those from all other alcoves (which may
538 include some rocks, as in the case of boulder-rich mantles).

539 Among flows that moved boulders, the median size of the largest transported
540 boulder is 1 m. Among flows that buried boulders in deposits near their terminus, the
541 median size of the largest buried boulder was also 1 m. This suggests that in the largest
542 gully flows, the thickest parts of the active flow and of the final deposits are at least 1 m
543 thick. The largest boulder observed to move was a 5-meter boulder that fell from the lip
544 of a retreating alcove head scarp (Fig. 8).

545 Thin flows could be several centimeters thick while having no topographic relief
546 visible to HiRISE. This is not precisely quantifiable. The horizontal pixel scale of
547 HiRISE data is 25–30 cm, but vertical changes equal to a fraction of the pixel dimension
548 would create slopes and topographic shading if they occur over short horizontal
549 baselines. There is little constraint on the lower bound other than that the deposit must be
550 thick enough to change the albedo of the surface, which can be as little as tens of microns
551 (e.g., Wells et al., 1984; Fischer and Pieters, 1993). Overprinting of repeated thin flows in
552 one gully in Ariadnes Colles (Fig. 6) demonstrates that the deposits are not thick enough
553 to deflect similar subsequent flows, but this does not directly constrain the thickness since
554 it is also affected by flow momentum. However, given the existence of many flows with
555 resolvable topographic effects, it is likely that the thin-flow thicknesses are mostly just
556 below resolvable with HiRISE and include few-cm-scale topographic changes.

557 The active gullies also suggest a fining-downslope sequence. Of the studied
558 alcoves, 50% were cut into rock or a rock-mantle mixture, but only 22% of aprons had

559 more than a few sparse boulders on the surface. This may to some extent reflect post-
560 deposition modification (de Haas et al., 2015b), but most evidence for such modification
561 such as inverted channels standing in relief (de Haas et al., 2015b; Dickson et al., 2015)
562 suggests deflation, which would concentrate boulders at the surface.
563
564 *3.5. Non-flow changes*
565 The non-flow changes observed fall into two main categories. The first is albedo
566 halos observed around channels. In most cases these are associated with sandy material,
567 although the halos themselves can be bright or dark. These are likely to indicate minor
568 flows lacking any observable flow feature, and/or sliding CO_2 blocks throwing material
569 out of gullies; halos have been observed in direct association with CO_2 blocks in dune
570 gullies in Russell crater (Dundas et al., 2012; Diniega et al., 2013). The second category
571 is movement of individual boulders or minor mass wasting (Fig. 10) (Harrison et al.,
572 2015; Raack et al., 2020). These reflect small-scale mass movement that was too low-
573 volume or not mobile enough to create a recognizable flow. Examples of this have been
574 noted to occur in spring or summer (e.g., Fig. 10; Harrison et al., 2015), so unlike the
575 major flows this activity is not necessarily driven by CO_2 frost. Boulder movement on
576 non-gullied slopes has in some cases been observed in frost-free seasons and could have a
577 range of causes (Dundas et al., 2019b). As noted in section 2 this tabulation is certainly
578 incomplete, and based on the Hale crater example, likely to a large degree.
579
580 **4. Distribution of Gully Site Activity Frequencies**

581 Figure 5 shows the distribution of observed gully site activity frequencies. Such
582 data offer the prospect of understanding the true distribution of underlying frequencies of
583 activity on a per-site basis. The lower flow frequencies on this plot should not be affected
584 by the biases favoring observation of the most active sites. This section presents an initial
585 exploration of this topic which also demonstrates uncertainties and potential issues.
586 The data appear linear on a log-log plot (a power-law relationship) up to around
587 one flow per Mars year per site, rolling off to lower numbers of sites at higher rates.
588 Simple extrapolation of the power law in Fig. 5 (fit by eye, since the errors are not well-
589 defined) suggests that all sites would have an observed activity frequency exceeding the
590 lowest observable value once frequencies of one flow per site per 44 Mars years are
591 observable. (This is not likely to be literally true, given the limitations of real data and
592 sporadically active processes.) Surprisingly, the same analysis for the north (Fig. S1)
593 yields a similar value of one flow per site per 46 Mars years even though the number of
594 more-active sites is lower. This appears to suggest that the least-active present-day gullies
595 have frequencies of at least one flow per site per ~45 Mars years. This would translate to
596 individual gully flow frequencies on the order of one per thousand Mars years, although
597 it could be more often (shorter recurrence intervals) if the least-active sites have lower
598 average numbers of gullies. There are, however, very large uncertainties with this
599 estimate.
600 This approach requires extrapolation over an order of magnitude in the flow
601 frequency domain, and over 75% of the total number of sites. It is entirely possible that
602 there is a change in the physical controls within that range, such as a sub-population of
603 inactive gullies. This is the information of most interest and cannot be determined by

604 extrapolation. However, there is no observational evidence of such a sub-population to
605 date; this would appear as a flattening of the slope at low activity frequencies. A longer
606 observing time will be required to test for such a feature.
607 The occurrence of the down-turn at one flow per site per Mars year is surprising:
608 a site contains variable numbers of gullies with variable properties, and there is no reason
609 to expect this rate to have any special meaning. One possibility is that it reflects
610 quantization since both the number of flows and number of years of monitoring are low,
611 and most observed frequencies below 1/Mars year are of the form 1/N or 2/N where N is
612 a low integer. Since the survey only includes confirmed changes the error is always
613 quantized and always above the observed point, and some sites with one or two flows
614 would have more if all changes were perfectly observed. The number of sites at or above
615 a given frequency is independent of this, however, so the down-turn is likely a real
616 feature.
617 Although we have emphasized the uncertainties above, collection of this survey
618 opens the door to analysis of population statistics for gully flows and activity rates. We
619 note here a few factors that should be considered as such analyses develop. The data are
620 an under-count of the total number of current gully flows, as discussed in Section 2.
621 Current survey methods are most likely to miss small flows or those which do not
622 descend to the apron. This incompleteness should be reduced in the future as orthoimages
623 with excellent lighting matches become available for more sites, and it may eventually be
624 possible to conduct broad surveys with such data. A key unknown is the extent to which
625 reducing this incompleteness will increase the number of active sites, as opposed to the
626 number of flows at the known active sites—in other words, the true curve in Fig. 5 would

627 be higher with perfect data, but how the slope will change is uncertain. Measurement of
628 flow volumes is presently challenging (Sutton et al., 2015), but an obvious area of
629 interest; any future investigation of a flow magnitude-frequency relationship will need to
630 consider incompleteness, particularly at small sizes. On Earth, both debris flows (e.g.,
631 Riley et al., 2013) and rockfalls (e.g., Williams et al., 2019) have magnitude-frequency
632 distributions that can be described by power laws, so this is a reasonable working
633 hypothesis for Martian gully flows. If this hypothesis is correct, the relative lack of thin
634 flows in the present data suggests significant observational incompleteness for the
635 smallest flows. Otherwise, this suggests a minimum flow thickness needed to descend the
636 full gully system. Observational incompleteness is favored because we know that there
637 are small flows (cf. de Haas et al., 2019b) and flows visible only in shadow, or with
638 minimal visible effect after frost sublimation (Fig. 3), which must commonly be missed
639 at the many sites where winter images were not acquired. However, both factors may
640 play a role. An additional challenge is that the occurrence of multiple flows in individual
641 gullies in several cases means that for sites with multiyear separation between images,
642 multiple flows might appear as one event; this is a known challenge for terrestrial rockfall
643 magnitude-frequency studies (e.g., Williams et al., 2019) although likely less acute for
644 rarer events like gully flows.

645 The distribution of lower frequencies can be described by a power law, but the
646 underlying statistics are likely better described by independent Poisson distributions of
647 events for each site. The number of flows in any one year at any one site may be
648 described to first order by a Poisson distribution. A Poisson distribution requires that
649 events be independent, which is not strictly true since one flow in a gully likely alters

conditions in ways that change the probability of future flows. Since most sites include many gullies this is likely a second-order effect but the strength remains to be determined. However, each gully site will have a different Poisson parameter (mean number of flows per year); this is likely also different for each individual gully, with the site mean reflecting the sum of the means for the individual gullies. Fig. 5 reflects an approximation of the distribution of those individual means, which encompass both variations in the number of gullies and the per-gully activity rate. This may provide the basis for further analysis of gully flow frequencies beyond the scope of this paper.

5. Interpretation and Discussion

5.1. Sediment transport and gully formation

If CO_2 processes like those operating at present are responsible for gully formation, the sediment transported by the current flows should be comparable to that on the fans, and the gully properties should be linked to the flow properties. Our observations are consistent with this. Present-day flows regularly transport boulders within the gully system. Flows are more likely to transport boulders when the alcove is rocky, and also when the apron is rocky. This is fully consistent with the hypothesis that current processes are sufficient to transport the appropriate range of particle sizes through gully systems and deposit them on the fans, and thus to drive gully formation. This may appear at odds with the observation by de Haas et al. (2015b) that channel walls were more likely to show boulders than fan surfaces, which could suggest a change over time. However, in a system with variable flow sizes it is unlikely that the most recent flow has been the largest. The largest events are more likely to be reflected in the stratigraphy.

673 Additionally, we observe that major flows are more likely to be associated with well-
674 developed alcoves. This is expected if present-day processes are those responsible for
675 gully formation since more erosion is required to create the larger recesses; a different
676 flow frequency could also contribute.

677 There have been suggestions that present-day flows are incapable of eroding
678 bedrock or solid ice as required for some gully alcoves (Dickson et al., 2021; Khuller and
679 Christensen, 2021), and that therefore aqueous flows should be preferred as a gully
680 formation mechanism. It is likely that some erosion of either substrate can occur at the
681 base of a CO_2-charged granular flow, as this occurs in both wet and dry granular flows
682 (e.g., Hsu et al., 2008). However, there is no need for such flows to directly erode most of
683 the alcove volume of coherent rock or ice for them to be the major agent forming gullies.
684 Additional mechanisms may break down material in the alcove for transport; flows will
685 scour the loose debris and in some cases also erode the coherent material along the flow
686 path in the deepest part of the alcove. This is a very common sediment cascade for debris
687 flows on Earth, where bedrock is weathered in place, transported into the channel
688 network by mass wasting (e.g., rockfalls and small landslides) and then mobilized by
689 debris flows (e.g., Larsen et al., 2006; Tang et al., 2009).

690 Breakdown of bedrock could be driven by numerous processes such as thermal
691 cycling, ice lens growth, or aeolian abrasion; all three processes are likely occurring on
692 present-day Mars (e.g., Viles et al., 2010; Bridges et al., 2012; Sizemore et al., 2015).
693 Small amounts of past liquid water could also have contributed to rock breakdown (e.g.,
694 Head et al., 2011; Conway et al., 2018). Experimentally, the strength of basalt blocks was
695 reduced by ~1% after only 36 Mars-like temperature cycles (Viles et al., 2010), and

696 thermal stress appears to be the driver of recent rockfalls on Mars (e.g., Tesson et al.,
697 2020), suggesting that typical thermal cycling on the Martian surface is an important
698 rock-breakdown process. Khuller and Christensen (2021) dismissed this effect because
699 boulders exist on old surfaces in equatorial regions, but rockfalls are an ongoing process
700 there (Dundas et al., 2019b; Grindrod et al., 2021; Vijayan et al., 2022); moreover, the
701 presence of surface or near-surface H_2O ice and CO_2 frost may enhance rock breakdown
702 in the mid-latitudes. Thermal stresses may be particularly strong immediately after
703 removal of seasonal CO_2 frost. Rock breakdown by ice lens growth has been reported on
704 Earth (e.g., Mackay, 1999), and while growth of Martian ice lenses may be slower
705 (Sizemore et al., 2015) it could be an effective agent in some circumstances. Sand
706 saltation is active planet-wide on Mars (Bridges et al., 2013); while the fluxes suggest
707 that abrasion only occurs at ~10 microns per year (Bridges et al., 2012), this may
708 contribute to forcing open cracks and removing material loosened by other processes.
709 Gullies appear to transport material without mineralogical alteration (Núñez et al., 2016)
710 so there is no evidence that chemical weathering or mineral hydration contribute
711 significantly to rock breakdown in alcoves, but if the surface of the alcove material is as
712 weathered as the apron then it could also be occurring to some extent.
713 Sublimation/erosion cycles are a predictable consequence of the physics of water
714 ice in the Martian mid-latitudes. Ice that is too shallow will sublimate, freeing up debris
715 that can be eroded when on steep slopes, and repeated occurrences of this cycle can
716 iteratively create a large gully. Surface water ice in the Martian mid-latitudes is unstable
717 and is found beneath a sublimation lag that thermally stabilizes it; such a cover may be
718 millimeters to meters thick depending on slope, aspect, and latitude (e.g., Mellon et al.,

719 2004; Aharonson and Schorghofer, 2006). Observations of rocks falling from a pole-
720 facing ice slope at 55 °S indicate that bare ice sublimates millimeters per Mars year under
721 those conditions (Dundas et al., 2018); a lag must be several centimeters thick to
722 significantly slow sublimation under Martian conditions (Schorghofer, 2020) and retreat
723 will continue until the ice is at its equilibrium depth. It is thus expected that a loose
724 sublimation lag centimeters thick can accumulate on short timescales if the debris above
725 ice is removed by a gully flow.

726 This process allows iterative erosion of a gully system without directly eroding
727 ice, in a manner similar to that suggested by Pilorget and Forget (2016). Flows are
728 directed into the thalweg of a developing system, so loose debris (whether freed by
729 sublimation or left behind by other recent flows) is most frequently removed there. This
730 means that sublimation is most rapid, deepening the thalweg path. Incision of discrete
731 channels occurs in the fines and debris of the apron, or in transient loose material
732 occupying the floor of the alcove. Some gullies could evolve to a state with a thicker
733 cover of debris on the alcove floor, which may host channels but cease significant down-
734 cutting except after the largest flows. The upper alcove expands by sublimation but
735 without the focusing process that occurs along the thalweg, giving alcoves in mantle
736 material morphologies that resemble scalloped depressions formed via sublimation
737 (Dundas et al., 2015a). Broad pits observed in mantle deposits on some crater walls
738 (Jawin et al., 2018) represent the same process with few or no CO_2-triggered flows to
739 sweep material down the slope. Evolution of gully alcoves in rocky material is similar but
740 with rock breakdown processes substituting for sublimation.

741 In this model, there should be considerable ongoing precursor activity in gully
742 alcoves, in addition to the CO_2-charged flows that sweep the debris down the gully
743 system. This predicted sequence of alcove collapses followed by larger flows has been
744 directly documented in a dune gully in Matara crater (Pasquon et al., 2019a). Much of the
745 precursor activity may be subtler in non-dune gullies, but evidence for such activity has
746 emerged within the last few years. Both Dundas et al. (2019a) and Khuller and
747 Christensen (2021) reported changing exposures of bright material in gully alcoves,
748 which they interpreted as evidence of ice being exposed. Khuller and Christensen (2021)
749 also reported a variety of topographic changes in an alcove in Dao Vallis, which did not
750 propagate a significant flow down the gully system. Harrison et al. (2015) noted fresh
751 rockfalls in alcoves in Gasa crater, and the compilation of de Haas et al. (2019b) for their
752 study site in Hale crater includes many examples of small slumps, short striations on
753 alcove walls, and short-range boulder movement. The non-flow events in Table S2 (e.g.,
754 Fig. 10) add further evidence for such processes. Such small-scale breakdown processes
755 need not be confined to the winter season, and H_2O sublimation would occur in the spring
756 and summer.
757 In this framework, gullies should be understood as sediment-transport systems
758 produced by many events, analogous to debris-flow catchments on Earth (e.g., Simoni et
759 al., 2020). The channels are dynamic features that repeatedly undergo partial infill by
760 low-energy or waning flows (or in low-velocity reaches) and aeolian processes, only to
761 be removed by later events. This can manifest as either near-complete infill and
762 reactivation, or as smaller sediment bodies that are deposited and removed within larger
763 channels. We have observed evidence of both: parts of the event in Fig. 2 appear to

764 reactivate nearly buried channels, while the distributed deposition and removal observed
765 in many channels indicates temporary deposition and removal of small sediment masses.
766 At the largest scale, channel breakouts may lead to anastomosis, and old buried channels
767 may become the preferred pathways for breakouts. Fig. 7 shows both removal of infill
768 within a blocked channel, and extension of the channel into a region where no prior
769 incision is apparent.
770
771 *5.2. Frequency of gully flows*
772 The results of this survey reinforce those of previous work (Dundas et al., 2012;
773 2015b; 2019a; Raack et al., 2020): Martian gully activity is substantial. Typical flow
774 recurrence intervals in any given cluster of gullies are decades, and are centuries for any
775 individual gully. Obliquity values have been within 3° of present values for over 300 kyr
776 (Laskar et al., 2004) and the atmospheric pressure has likely been within ~25% of the
777 present value for the last 200 kyr (Bierson et al., 2016; Buhler et al., 2020). The major
778 source of climate variations over that interval is changes in the season of perihelion,
779 which affects the relative intensity of seasons. Currently, the southern hemisphere
780 experiences warmer summers and longer, colder winters than the north, which may
781 prevent activity in the lowest-latitude northern gullies, but this should reverse on ~25 kyr
782 timescales. If this is the cause of the current hemispheric difference in activity frequency,
783 it should also reverse. Regardless, unless there is a group of entirely inactive gully
784 landforms it is likely that most individual gullies have experienced dozens if not
785 hundreds of individual flows in a climate much like the present. The most active gullies
786 have experienced thousands of flows.

This level of activity is sufficient to fully account for gully formation in reasonable timescales. Istok crater provides an excellent case study because it has an estimated age of 0.19 Ma (Johnsson et al., 2014), entirely within the recent period of relative climate stability. De Haas et al. (2015a) estimated that formation of the group of gullies in Istok involved ~28,000 "modal-sized" debris flows, or one flow every 3.6 Mars years. We have documented one major flow similar to their modal flows, plus two thin flows, in two Mars years of good coverage. (HiRISE coverage of Istok spans six winter solstices, but the earliest images have deep shadows over many of the gullies so only two years are bracketed by good-quality data.) Within the large uncertainties on each estimate, this is good agreement. Older systems may be expected to have more complex and variable histories stretching back millions of years. For example, Gasa crater has an estimated age of 1.25 Ma, and activity in Artik crater both pre- and post-dates formation of Gasa (Schon et al., 2009). Notably, the well-developed gullies of Gasa crater are among the most active on Mars, and activity in Artik is ongoing as well. Rates may certainly have varied but this chronostratigraphic evidence does not require that other processes be invoked. Indeed, it would be surprising if there was a second set of processes that produced such similar morphological outcomes.

Several gullies have experienced multiple individual flows (e.g., Fig. 7). Such a high frequency of flows could indicate extremely rapid gully formation, which is likely the case for some dune gullies (Diniega et al., 2010; Dundas et al., 2019a; Pasquon et al., 2019b). However, for non-dune gullies with more coherent substrates and less dynamic surfaces, the high frequency of flows may indicate that an initial flow facilitates subsequent flows for some interval by disturbing the surface and removing support from

other slopes that subsequently fail. This type of feedback effect may influence some of the most-active non-dune gully sites (section 3.2) with the highest frequencies (Fig. 5), but is not the sole cause of those high frequencies since most of those sites show activity in many individual gullies. It is unknown at present how the frequency of flows in an individual gully varies over time.

The reason for the wide variation of gully activity frequencies is unknown. The geologic and climatologic properties that yield high activity levels are obscure at present, as discussed in section 3.2; sandy substrates and fresh crater slopes may be particularly favorable settings but are not required. Dundas et al. (2015b) found no obvious controls from multi-km scale albedo, elevation, or thermal inertia. It is likely that the controls relate to very local properties: slope and aspect, frost abundance and defrosting behavior, lithology, rock strength, regolith thickness and cohesion, and depth to ice, at the scale of individual gully landforms or even individual alcove reaches. Number of gullies or gullied slope area must also affect the frequency on a site-by-site basis.

The fresh appearance of most gullies, and the continuing rise in the fraction of active monitoring sites as time baselines extend (Fig. 4), are consistent with few if any inactive gullies. It will not be possible to distinguish between inactive gullies and those with recurrence intervals of centuries for some time. However, the rise of the curves in Fig. 4 must ultimately flatten, as it will require ever-longer observation intervals to include the least-active gullies. It should eventually be possible to determine whether the active fraction is asymptotically approaching some fraction <1. The key observation will be whether the activity-frequency curve (Fig. 5) eventually flattens at low frequencies as more data are acquired. It is likely that the lowest-latitude northern gullies are inactive at

present, as the shorter northern winter does not allow frost to reach the lowest latitudes, but this will reverse over the next ~25 kyr.

These data have implications for possible future observations of gullies. The data set used here reflects no more than 6 and 7 winter solstices for the longest HiRISE series in the south and north, respectively, and more than an additional Mars year of data has been collected but not analyzed at the time of publication. If extrapolation of the power laws in Figs. 5 and S2 is close to accurate, half of all gully sites in the southern hemisphere would have observed activity after 18 Mars years of monitoring, and 80% after 33 Mars years. In the north, the corresponding values are 26 and 38 Mars years. These extrapolations are not predictions but instead suggest the approximate observing timescales required to test for roll-off in Fig. 5 indicating an inactive fraction of ~50% or ~20%. The timescales could be somewhat shorter, since our observations are a lower bound on activity and some sites have only low-quality data. A long-term presence of HiRISE-class orbital imaging would be required to make such observations. Additionally, the most active locations have a >50% chance of a flow event in any one Martian winter, raising the possibility that a landed mission could be designed to observe one.

6. Conclusions

Hundreds of flows have occurred in Martian gullies within the last 15 years. These flows are driven by CO_2 frost, although smaller-scale precursor activity in the form of dry mass wasting can occur in frost-free seasons. Gully sites have a range of flow frequencies, which can be characterized by a power law that rolls off at the highest frequencies. Some sites (comprised of multiple gullies) have flows occurring nearly every

Mars year and some individual gullies have been repeatedly active within a few Mars years, while events in other gullies are orders of magnitude less frequent. The flow frequency in the least-active sites cannot currently be measured, but there is no evidence that any substantial fraction of gullies are totally inactive. It is possible that the least-active gullies have current flow recurrence intervals of a few hundred to a few thousand Mars years, which implies hundreds of individual flows since the last period of high-obliquity when snow and frost accumulation is thought to have occurred; the lowest-latitude northern gullies may be currently inactive due to the timing of aphelion but this changes on 25-kyr timescales. Sediment transport in gullies is substantial and consistent with ongoing formation, as rock transport is more common in flows where the eroded material of the alcove is rock. While a past role for liquid water cannot be ruled out, the nature and frequency of current activity are consistent with CO_2 frost processes as the driver forming gullies, and nearly preclude good preservation of morphologies from past high-obliquity periods.

Acknowledgments

CMD and GEC were funded by Mars Data Analysis Program agreement 80HQTR19T0087. SJC is funded for her HiRISE work by the French Space Agency, CNES. HiRISE targeting and imaging was funded by the Mars Reconnaissance Orbiter project. HiRISE RDR observations were collected and processed by NASA/JPL/University of Arizona and are available via the Planetary Data System (https://hirise-pds.lpl.arizona.edu/PDS/) and tables of monitoring sites and changes are available as a USGS data release (Dundas, 2020; https:// doi.org/10.5066/P9IXL0XT).

Jay Dickson and an anonymous referee provided helpful reviews and Kaj Williams provided comments on an early draft. Discussions with Serina Diniega, Alfred McEwen, Shane Byrne, and Candice Hansen have been very helpful. Nicole Baugh and Christian Schaller developed software tools used to plan "HiKER" observations. Kelly Pasquon, Lujendra Ojha, Sara Martínez-Alonso, and Virginia Gulick called attention to individual flows included here, and the MRO CTX team has suggested some locations of possible activity for HiRISE imaging. Any use of trade, firm, or product names is for descriptive purposes only and does not imply endorsement by the U.S. Government.

References

Aharonson, O., Schorghofer, N. (2006). Subsurface ice on Mars with rough topography. J. Geophys. Res., 111, E11007. https://doi.org/10.1029/2005JE002636.

Aston, A. H., Conway, S. J., Balme, M. R. (2011). Identifying Martian gully evolution. Geol. Soc. London Spec. Pub., 356, 151-169. https://doi.org/10.1144/SP356.9.

Bierson, C. J., Phillips, R. J., Smith, I. B., Wood, S. E., Putzig, N. E., Nunes, D., Byrne, S. (2016). Stratigraphy and evolution of the buried CO2 deposit in the Martian south polar cap. Geophys. Res. Lett., 43. https://doi.org/10.1002/2016GL068457.

Bridges, N. T., Ayoub, F., Avouac, J.-P., Leprince, A., Mattson, S. (2012). Earth-like sand fluxes on Mars. Nature, 485, 339-342. https://doi.org/10.1038/nature11022.

Buhler, P. B., Ingersoll, A. P., Piqueux, S., Ehlmann, B. L., Hayne, P. O. (2020). Coevolution of Mars's atmosphere and massive south polar CO_2 ice deposit. Nature Astron., 4, 364-371. https://doi.org/10.1038/s41550-019-0976-8.

Christensen, P.R. (2003). Formation of recent Martian gullies through melting of extensive water-rich snow deposits. Nature, 422, 45-48. https://doi.org/10.1038/nature01436.

Bridges, N., Geissler, P., Silvestro, S., Banks, M. (2013). Bedform migration on Mars: Current results and future plans. Aeolian Res., 9, 133-151. https://doi.org/10.1016/j.aeolia.2013.02.004.

Clancy, R.T., Sandor, B.J., Wolff, M.J., Christensen, P.R., Smith, M.D., Pearl, J.C., Conrath, B.J., Wilson, R.J. (2000). An intercomparison of groundbased millimeter, MGS TES, and Viking atmospheric temperature measurements: Seasonal and interannual variability of temperatures and dust loading in the global Mars atmosphere. J. Geophys. Res., 105, 9553–9572. https://doi.org/10.1029/1999JE001089.

Conway, S. J., Balme, M. R. (2014). Decameter thick remnant glacial ice deposits on Mars. Geophys. Res. Lett., 41, 5,402-5,409. https://doi.org/10.1002/2014GL060314.

Conway, S. J., Butcher, F. E. G., de Haas, T., Deijns, A. A. J., Grindrod, P. (2018). Intense glacial erosion could have erased gullies on Mars. Lunar Planet. Sci. Conf. 49, abstract #1875.

Conway, S. J., de Haas, T., Harrison, T. N. (2019). Martian gullies: a comprehensive review of observations, mechanisms and insights from Earth analogues. Geol. Soc. London Spec. Pub., 467, 7-66. https://doi.org/10.1144/SP467.14.

Costard, F., Forget, F., Mangold, N., Peulvast, J. P. (2002). Formation of recent Martian debris flows by melting of near-surface ground ice at high obliquity. Science, 295, 110-113. https://doi.org/10.1126/science.1066698.

924 de Haas, T., Hauber, E., Conway, S. J., van Steijn, H., Johnsson, A., Kleinhans, M. G.
925 (2015a). Earth-like aqueous debris-flow activity on Mars at high orbital obliquity in
926 the last million years. Nature Commun., 6:7543.
927 https://doi.org/10.1038/ncomms8543.
928 de Haas, T., Ventra, D., Hauber, E., Conway, S. J., Kleinhans, M. G. (2015b).
929 Sedimentological analyses of Martian gullies: The subsurface as the key to the
930 surface. Icarus, 258, 92-108. https://doi.org/10.1016/j.icarus.2015.06.017.
931 de Haas, T., Conway, S. J., Butcher, F. E. G., Levy, J., Grindrod, P. M., Goudge, T. A.,
932 Balme, M. R. (2019a). Time will tell: Temporal evolution of Martian gullies and
933 palaeoclimatic implications. Geol. Soc. London Spec. Pub., 467, 165-186.
934 https://doi.org/10.1144/SP467.1.
935 de Haas, T., McArdell, B. W., Conway, S. J., McElwaine, J. N., Kleinhans, M. G.,
936 Salese, F., Grindrod, P. M. (2019b). Initiation and flow conditions of contemporary
937 flows in Martian gullies. J. Geophys Res. Planets, 124, 2,246-2,271.
938 https://doi.org/10.1029/2018JE005899.
939 Delamere, W. A., et al. (2010). Color imaging of Mars by the High Resolution Imaging
940 Science Experiment (HiRISE). Icarus, 205, 38-52.
941 https://doi.org/10.1016/j.icarus.2009.03.012.
942 Dickson, J. L., Head, J. W., Goudge, T. A., Barbieri, L. (2015). Recent climate cycles on
943 Mars: Stratigraphic relationships between multiple generations of gullies and the
944 latitude dependent mantle. Icarus, 252, 83-94.
945 https://doi.org/10.1016/j.icarus.2014.12.035.

946 Dickson, J. L., Palumbo, A. M., Kerber, L. A., Fassett, C. I., Kreslavsky, M. A. (2021).
947 The elevation distribution of mid-latitude gullies on Mars as a test of CO_2 and H_2O
948 formation and modification processes. Lunar Planet. Sci. Conf. 52, abstract #2426.
949 Diniega, S., Byrne, S., Bridges, N. T., Dundas, C. M., McEwen, A. S. (2010). Seasonality
950 of present-day Martian dune-gully activity. Geology, 38, 1047-1050.
951 https://doi.org/10.1130/G31287.
952 Diniega, S., Hansen, C.J., McElwaine, J.N., Hugenholtz, C.H., Dundas, C.M., McEwen,
953 A.S., Bourke, M.C. (2013). A new dry hypothesis for the formation of Martian linear
954 gullies. Icarus, 225, 526-537. https://doi.org/10.1016/j.icarus.2013.04.006.
955 Dundas, C. M. (2021). Dry formation of recent Martian slope features. In: Mars
956 Geological Enigmas From the Late Noachian Epoch to the Present Day (R. Soare, S.
957 Conway, J.-P. Williams, & D. Oehler (eds.)), Elsevier Books, Amsterdam, p. 263-
958 288. https://doi.org/10.1016/B978-0-12-820245-6.00010-0.
959 Dundas, C. M. (2022). Gully monitoring sites and new flows on Mars observed in
960 HiRISE data. U.S. Geological Survey Data Release.
961 https://doi.org/10.5066/P9IXL0XT.
962 Dundas, C. M., McEwen, A.S., Diniega, S., Byrne, S., Martinez-Alonso, S. (2010). New
963 and recent gully activity on Mars as seen by HiRISE. Geophys. Res. Lett., 37,
964 L07202. https://doi.org/10.1029/2009GL041351.
965 Dundas, C. M., Diniega, S., Hansen, C.J., Byrne, S., McEwen, A.S. (2012). Seasonal
966 activity and morphological changes in Martian gullies. Icarus, 220, 124-143.
967 https://doi.org/10.1016/j.icarus.2012.04.005.

968 Dundas, C. M., Byrne, S., McEwen, A. S. (2015a). Modeling the development of Martian
969 sublimation thermokarst landforms. Icarus, 262, 154-169.
970 https://doi.org/10.1016/j.icarus.2015.07.033.
971 Dundas, C. M., Diniega, S., McEwen, A. S. (2015b). Long-term monitoring of Martian
972 gully formation and evolution with MRO/HiRISE. Icarus, 251, 244-263.
973 https://doi.org/10.1016/j.icarus.2014.05.013.
974 Dundas, C. M., et al. (2018). Exposed subsurface ice sheets in the Martian mid-latitudes.
975 Science, 359, 199-201. https://doi.org/10.1126/science.aao1619.
976 Dundas, C. M., McEwen, A. S., Diniega, S., Hansen, C. J., Byrne, S., McElwaine, J. N.
977 (2019a). The formation of gullies on Mars today. Geol. Soc. London Spec. Pub., 467,
978 67-94. https://doi.org/10.1144/SP467.5.
979 Dundas, C. M., Mellon, M. T., Conway, S. J., Gastineau, R. (2019b). Active boulder
980 movement at high Martian latitudes. Geophys. Res. Lett., 46, 5,075-5,082.
981 https://doi.org/10.1029/2019GL082293.
982 Fischer, E. M., Pieters, C. M. (1993). The continuum slope of Mars: Bidirectional
983 reflectance investigations and applications to Olympus Mons. Icarus, 102, 185-202.
984 https://doi.org/10.1006/icar.1993.1043.
985 Grindrod, P. M., Davis, J. M., Conway, S. J., de Haas, T. (2021). Active boulder falls in
986 Terra Sirenum, Mars: Constraints on timing and causes. Geophys. Res. Lett., 48,
987 e2021GL094817. https://doi.org/10.1029/2021GL094817.
988 Gulick, V. C., Glines, N., Hart, S., Freeman, P. (2019). Geomorphological analysis of
989 gullies on the central peak of Lyot crater, Mars. Geol. Soc. London Spec. Pub., 467,
990 233-265. https://doi.org/10.1144/SP467.17.

Hansen, C. J., Bourke, M., Bridges, N. T., Byrne, S., Colon, C., Diniega, S., Dundas, C., Herkenhoff, K., McEwen, A., Mellon, M., Portyankina, G., Thomas, N. (2011). Seasonal erosion and restoration of Mars' northern polar dunes. Science, 331, 575-578. https://doi.org/10.1126/science.1197636.

Harrison, T. N., Malin, M. C., Edgett, K. S. (2009). Liquid water on the surface of Mars today: Present gully activity observed by the Mars Reconnaissance Orbiter (MRO) and Mars Global Surveyor (MGS) and direction for future missions. AGU Fall Meeting, abstract #P43D-1454.

Harrison, T. N., Osinski, G. R., Tornabene, L. L., Jones, E. (2015). Global documentation of gullies with the Mars Reconnaissance Orbiter Context Camera and implications for their formation. Icarus, 252, 236-254. https://doi.org/10.1016/j.icarus.2015.01.022.

Head, J. W., Kreslavsky, M. A., Marchant, D. R. (2011). Pitted rock surfaces on Mars: A mechanism of formation by transient melting of snow and ice. J. Geophys. Res., 116, E09007. https://doi.org/10.1029/2011JE003826.

Hoffman, N. (2002). Active polar gullies on Mars and the role of carbon dioxide. Astrobiology, 2, 313–323. https://doi.org/10.1089/153110702762027899.

Hsu, L., Dietrich, W. E., Sklar, L. S. (2008). Experimental study of bedrock erosion by granular flows. J. Geophys. Res., 113, F02001. https://doi.org/10.1029/2007JF000778.

Ishii, T., Sasaki, S. (2004). Formation of recent Martian gullies by avalanches of CO_2 frost. Lunar Planet. Sci. Conf. 35, abstract #1556.

1012 Jawin, E. R., Head, J. W., Marchant, D. R. (2018). Transient post-glacial processes on
1013 Mars: Geomorphologic evidence for a paraglacial period. Icarus, 309, 187-206.
1014 https://doi.org/10.1016/j.icarus.2018.01.026.
1015 Johnsson, A., Reiss, D., Hauber, E., Hiesinger, H., Zanetti, M. (2014). Evidence for very
1016 recent melt-water and debris flow activity in gullies in a young mid-latitude crater on
1017 Mars. Icarus, 235, 37-54. https://doi.org/10.1016/j.icarus.2014.03.005.
1018 Khuller, A. R., Christensen, P. R. (2021). Evidence of exposed dusty water ice within
1019 Martian gullies. J. Geophys. Res. Planets: Planets, 126, article e2020JE006539.
1020 https://doi.org/10.1029/2020JE006539.
1021 Larsen, I. J., Pederson, J. L., Schmidt, J. C. (2006). Geologic versus wildfire controls on
1022 hillslope processes and debris flow initiation in the Green River canyons of Dinosaur
1023 National Monument. Geomorphology, 81(1-2), 114-127.
1024 https://doi.org/10.1016/j.geomorph.2006.04.002.
1025 Laskar, J., Correia, A. C. M., Gastineau, M., Joutel, F., Levrard, B. (2004). Long term
1026 evolution and chaotic diffusion of the insolation quantities of Mars. Icarus, 170, 343-
1027 364. https://doi.org/10.1016/j.icarus.2004.04.005.
1028 Mackay, J. R. (1999). Cold-climate shattering (1974 to 1993) of 200 glacial erratics on
1029 the exposed bottom of a recently drained Arctic lake, western Arctic coast, Canada.
1030 Permafrost and Periglacial Processes, 10, 125-136.
1031 Malin, M.C., Edgett, K.S. (2000). Evidence for recent groundwater seepage and surface
1032 runoff on Mars. Science, 288, 2,330-2,335.
1033 https://doi.org/10.1126/science.288.5475.2330.

1034 Malin, M. C., Edgett, K. S., Posiolova, L. V., McColley, S. M., Noe Dobrea, E. Z.
1035 (2006). Present-day cratering rate and contemporary gully activity on Mars. Science,
1036 314, 1,573-1,577. https://doi.org/10.1126/science.1135156.
1037 McEwen, A.S., Eliason, E.M., Bergstrom, J.W., Bridges, N.T., Hansen, C.J., Delamere,
1038 W.A., Grant, J.A., Gulick, V.C., Herkenhoff, K.E., Keszthelyi, L., Kirk, R.L., Mellon,
1039 M.T., Squyres, S.W., Thomas, N., Weitz, C.M. (2007). Mars Reconnaissance
1040 Orbiter's High Resolution Imaging Science Experiment (HiRISE). J. Geophys. Res.,
1041 112, E05S02. https://doi.org/10.1029/2005JE002605.
1042 McEwen, A. S., Ojha, L., Dundas, C. M., Mattson, S. S., Byrne, S., Wray, J. J., Cull, S.
1043 C., Murchie, S. L., Thomas, N., Gulick, V. C. (2011). Seasonal flows on warm
1044 Martian slopes. Science, 333, 740-743. https://doi.org/10.1126/science.1204816.
1045 Mellon, M. T., Feldman, W. C., Prettyman, T. H. (2004). The presence and stability of
1046 ground ice in the southern hemisphere of Mars. Icarus, 169, 324-340.
1047 https://doi.org/10.1016/j.icarus.2003.10.022.
1048 Mustard, J. F., Cooper, C. D., Rifkin, M. K. (2001). Evidence for recent climate change
1049 on Mars from the identification of youthful near-surface ground ice. Nature, 412,
1050 411-414. https://doi.org/10.1038/35086515.
1051 Núñez, J. I., Barnouin, O. S., Murchie, S. L., Seelos, F. P., McGovern, J. A., Seelos, K.
1052 D., Buczkowski, D. L. (2016). New insights into gully formation on Mars:
1053 Constraints from composition as seen by MRO/CRISM. Geophys. Res. Lett., 43,
1054 8,893-8,902. https://doi.org/10.1002/2016GL068956.

1055 Pasquon, K., Gargani, J., Massé, M., Conway, S. J. (2016). Present-day formation and
1056 seasonal evolution of linear dune gullies on Mars. Icarus, 274, 195-210.
1057 https://doi.org/10.1016/j.icarus.2016.03.024.
1058 Pasquon, K., Gargani, J., Massé, M., Vincendon, M., Conway, S. J., Séjourne, A.,
1059 Jomelli, V., Balme, M. R., Lopez, S., Guimpier, A. (2019a). Present-day development
1060 of gully-channel sinuosity by carbon dioxide gas-supported flows on Mars. Icarus,
1061 329, 296-313. https://doi.org/10.1016/j.icarus.2019.03.034.
1062 Pasquon, K., Gargani, J., Nachon, M., Conway, S. J., Massé, M., Jouannic, G., Balme, M.
1063 R., Costard, F., Vincendon, M. (2019b). Are different Martian gully morphologies
1064 due to different processes on the Kaiser dune field? Geol. Soc. London Spec. Pub.,
1065 467, 145-164. https://doi.org/10.1144/SP467.13.
1066 Pilorget, C., Forget, F. (2016). Formation of gullies on Mars by debris flows triggered by
1067 CO2 sublimation. Nature Geosci., 9, 65-69. https://doi.org/10.1038/ngeo2619.
1068 Piqueux, S., Byrne, S., Kieffer, H. H., Titus, T. N., Hansen, C. J. (2015). Enumeration of
1069 Mars years and seasons since the beginning of telescopic exploration. Icarus, 251,
1070 332-338. https://doi.org/10.1016/j.icarus.2014.12.014.
1071 Raack, J., Reiss, D., Appéré, T., Vincendon, M., Ruesch, O., Hiesinger, H. (2015).
1072 Present-day seasonal gully activity in a south polar pit (Sisyphi Cavi) on Mars. Icarus,
1073 251, 226-243. https://doi.org/10.1016/j.icarus.2014.03.040.
1074 Raack, J., Conway, S. J., Heyer, T., Bickel, V. T., Philippe, M., Hiesinger, H., Johnsson,
1075 A., Massé, M. (2020). Present-day gully activity in Sisyphi Cavi, Mars - Flow-like
1076 features and block movements. Icarus, 350, article #113899.
1077 https://doi.org/10.1016/j.icarus.2020.113899.

1078 Reiss, D., Erkeling, G., Bauch, K.E., Hiesinger, H. (2010). Evidence for present day gully
1079 activity on the Russell crater dune field, Mars. Geophys. Res. Lett., 37, L06203.
1080 https://doi.org/10.1029/2009GL042192.
1081 Riley, K. L., Bendick, R., Hyde, K. D., Gabet, E. (2013). Frequency-magnitude
1082 distribution of debris flows compiled from global data, and comparison with post-fire
1083 debris flows in the western U.S. Geomorphology, 191, 118-128.
1084 https://doi.org/10.1016/j.geomorph.2013.03.008.
1085 Schon, S. C., Head, J. W. (2012). Gasa impact crater, Mars: Very young gullies formed
1086 from impact into latitude-dependent mantle and debris-covered glacier deposits?
1087 Icarus, 218, 459-477. https://doi.org/10.1016/j.icarus.2012.01.002.
1088 Schon, S. C., Head, J. W., Fassett, C. I. (2009). Unique chronostratigraphic marker in
1089 depositional fan stratigraphy on Mars: Evidence for ca. 1.25 Ma gully activity and
1090 surficial meltwater origin. Geology, 37, 207-210. https://doi.org/10.1130/G25398A.1.
1091 Schorghofer, N. (2020). Mars: Quantitative evaluation of Crocus melting behind
1092 boulders. Astrophys. J., 890, 49. https://doi.org/10.3847/1538-4357/ab612f.
1093 Simoni, A., Bernard, M., Berti, M., Boreggio, M., Lanzoni, S., Stancanelli, L. M.,
1094 Gregoretti, C. (2020). Runoff-generated debris flows: Observations of initiation
1095 conditions and erosion-deposition dynamics along the channel at Cancia (eastern
1096 Italian Alps). Earth Surf. Process. Landforms, 45, 3556-3571.
1097 https://doi.org/10.1002/esp.4981.
1098 Sizemore, H. G., Zent, A. P., Rempel, A. W. (2015). Initiation and growth of Martian ice
1099 lenses. Icarus, 251, 191-210. https://doi.org/10.1016/j.icarus.2014.04.013.

Sutton, S. S., Chojnacki, M., Kilgallon, A., HiRISE Team (2015). Precision and accuracy of simultaneously collected HiRISE Digital Terrain Models. Lunar Planet. Sci. Conf. 46, abstract #3010.

Tang, C., Zhu, J., Li, W. L., Liang, J. T. (2009). Rainfall-triggered debris flows following the Wenchuan earthquake. Bulletin of Engineering Geology and the Environment, 68(2), 187-194. https://doi.org/10.1007/s10064-009-0201-6.

Tesson, P.-A., Conway, S. J., Mangold, N., Ciazela, J., Lewis, S. R., Méje, D. (2020). Evidence for thermal-stress-induced rockfalls on Mars impact crater slopes. Icarus, 342, article #113503. https://doi.org/10.1016/j.icarus.2019.113503.

Vijayan, S., Harish, Kimi, K. B., Tuhi, S., Vigneshwaran, K., Sinha, R. K., Conway, S. K., Sivaraman, B., Bhardwaj, A. (2022). Boulder fall ejecta: Present day activity on Mars. Geophys. Res. Lett., 49, e2021GL096808. https://doi.org/10.1029/2021GL096808.

Viles, H., Ehlmann, B., Wilson, C. F., Cebula, T., Page, M., Bourke, M. (2010). Simulating weathering of basalt on Mars and Earth by thermal cycling. Goephys. Res. Lett., 37, L18201. https://doi.org/10.1029/2010GL043522.

Wells, E. N., Veverka, J., Thomas, P. (1984). Mars: Experimental study of albedo changes caused by dust fallout. Icarus, 58, 331-338. https://doi.org/10.1016/0019-1035(84)90079-4.

Williams, J. G., Rosser, N. J., Hardy, R. J., Brain, M. J. (2019). The importance of monitoring interval for rockfall magnitude-frequency estimation. J. Geophys. Res. Earth Surf., 124, 2841-2853. https://doi.org/10.1029/2019JF005225.

Zurek, R.W., Smrekar, S.E. (2007). An overview of the Mars Reconnaissance Orbiter (MRO) science mission. J. Geophys. Res., 112, E05S01. https://doi.org/10.1029/2006JE002701.

Figures and Captions

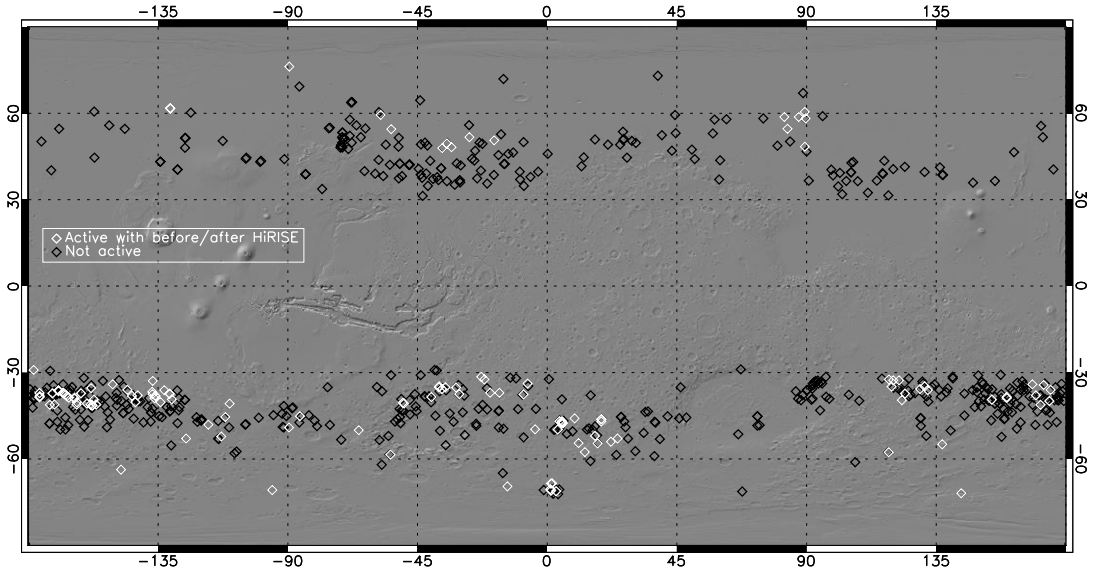

Figure 1. Map of monitoring sites (HiRISE image series) in this study (see table S1 for details). Background is shaded relief from the Mars Orbiter Laser Altimeter (MOLA) global Digital Elevation Model.

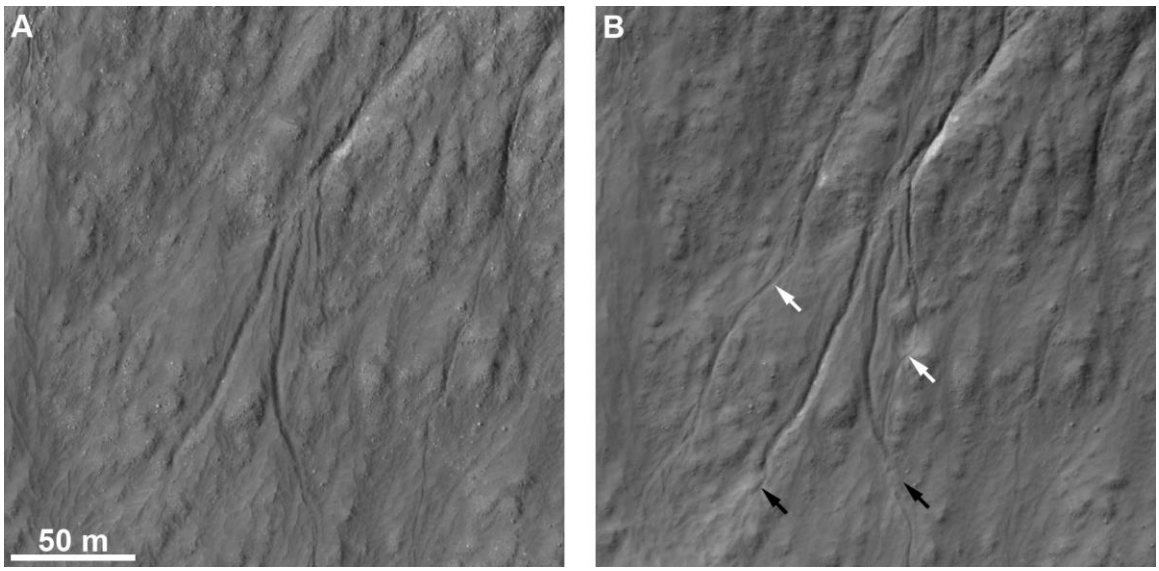

Figure 2: Incision of new channel reaches in a gully (36.7 ºS, 222.9ºE). White arrows indicate major incision and black arrows indicate deposition (Animation S1). North is up and downslope is towards the bottom in both panels. (All image figures are subsections

of HiRISE RDRs, which are created by NASA/JPL/University of Arizona and available via the Planetary Data System. Illumination is from the left in all figures. A: HiRISE image PSP_003094_1430. B: ESP_050538_1430.)

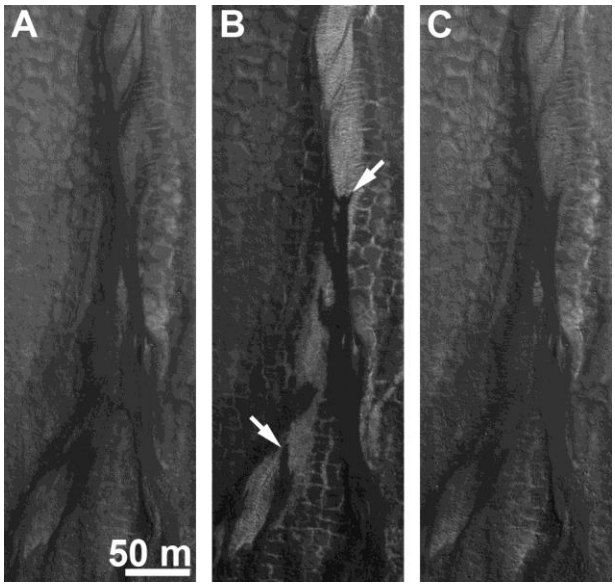

Figure 3: Fresh flow or flows (white arrows, B) in a gully (58.7ºN, 87.3ºE) which is not very apparent in comparing defrosted images before and after (A and C). Downslope and north are up in all panels. (A: ESP_025897_2390. B: ESP_059536_2390. C: ESP_060103_2390.)

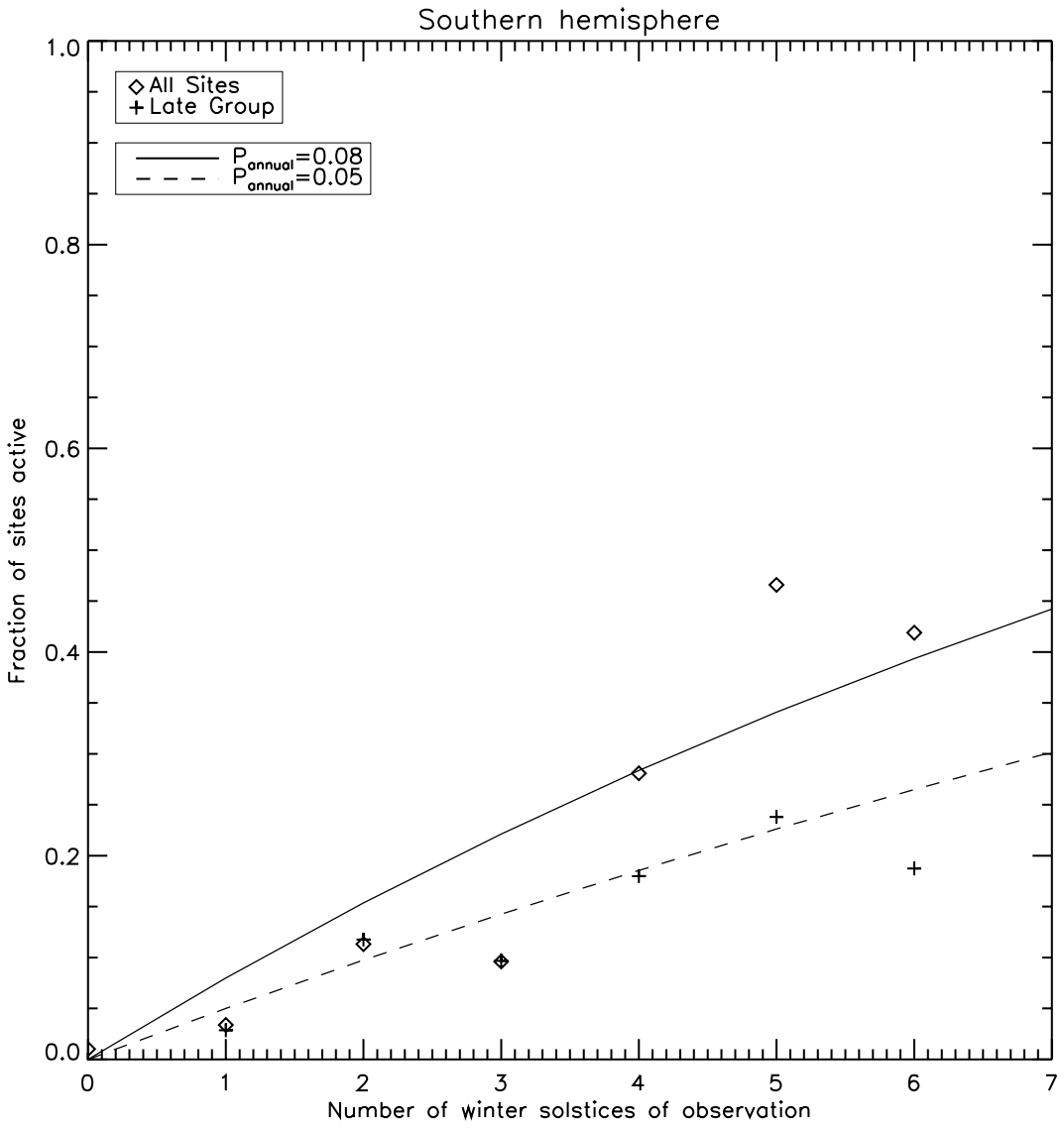

1145

1146 **Figure 4:** Fraction of gully sites (513 total sites across all bins) with observed activity as
1147 a function of the number of winter solstices spanned by monitoring images, for the
1148 southern hemisphere. Symbols show both the total data set (diamonds) and the most
1149 recently added monitoring sites, which should have reduced targeting biases. Curves
1150 show the expected fraction of sites that would be observed to be active if the probability
1151 of activity is 0.05 and 0.08 per winter.

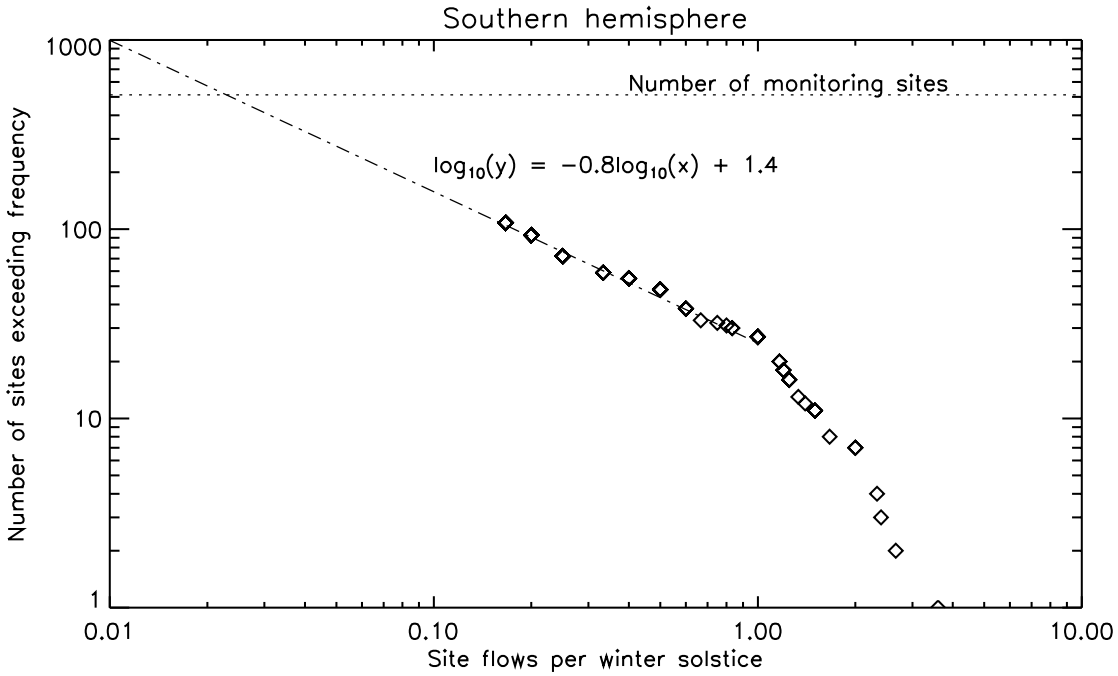

1152

1153 **Figure 5:** Cumulative plot of the number of gully sites with observed flow frequencies

1154 exceeding a given frequency, for the southern hemisphere. Power law fit is by eye and

1155 the extrapolation to lower frequencies may be inaccurate; it does not describe the higher

1156 frequencies well. See the discussion in section 4.

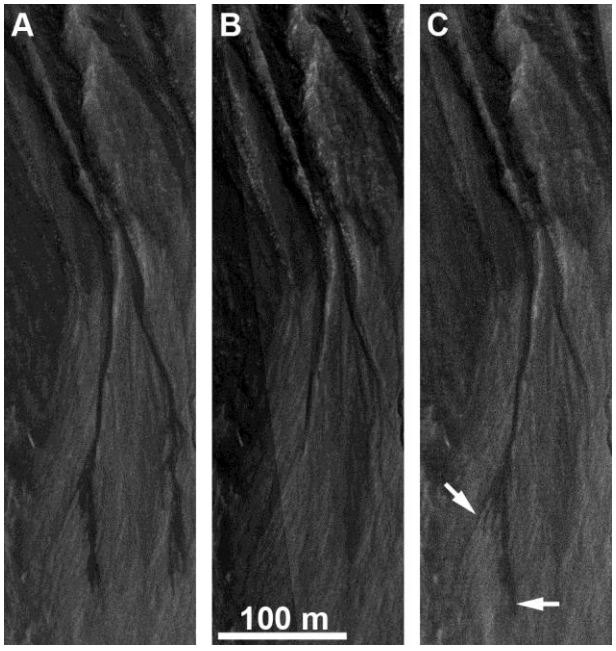

1157

Figure 6: Flows in shadow in Ariadnes Colles (34.4 ºS, 172.3 ºE). The pattern changes from winter to winter, demonstrating that these are active flows occurring in different gullies each year. One gully has similar flows in A and C; the flow in C is more extensive (arrows), so while it followed a similar flow path it is a separate flow. Downslope is down and north is up in all panels. (A: PSP_009161_1450. B: ESP_027002_1455. C: ESP_044105_1455. All images have been given a hard linear stretch to show details in dark shadows; data available via the PDS.)

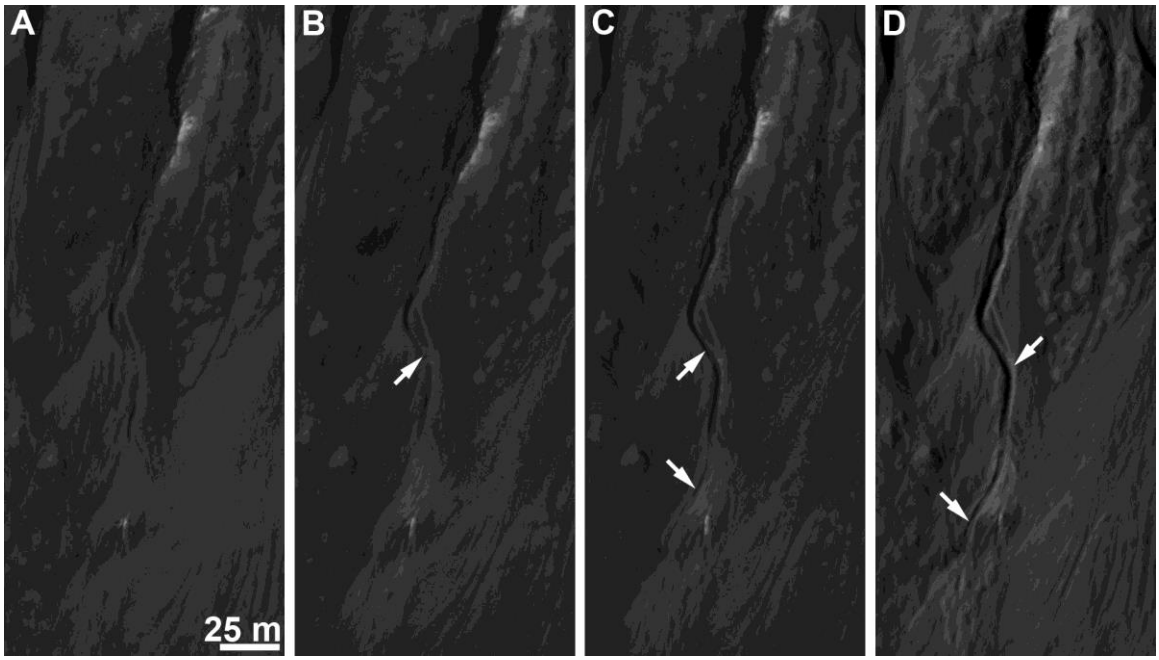

Figure 7: Example of multiple flows in an individual gully (36 ºS, 214.3 ºE) over several Mars years. The channel widened, deepened, and extended nearly 50 m. Arrows show notable locations of erosion. The first stage (B) may have removed material previously clogging the channel. Deposition occurred at lower left. A–C have similar illumination, while D has somewhat higher incidence angle. Downslope is down and north is up in all

panels. (A: ESP_014368_1435. B: ESP_031919_1435. C: ESP_039818_1435. D: ESP_055549_1435.)

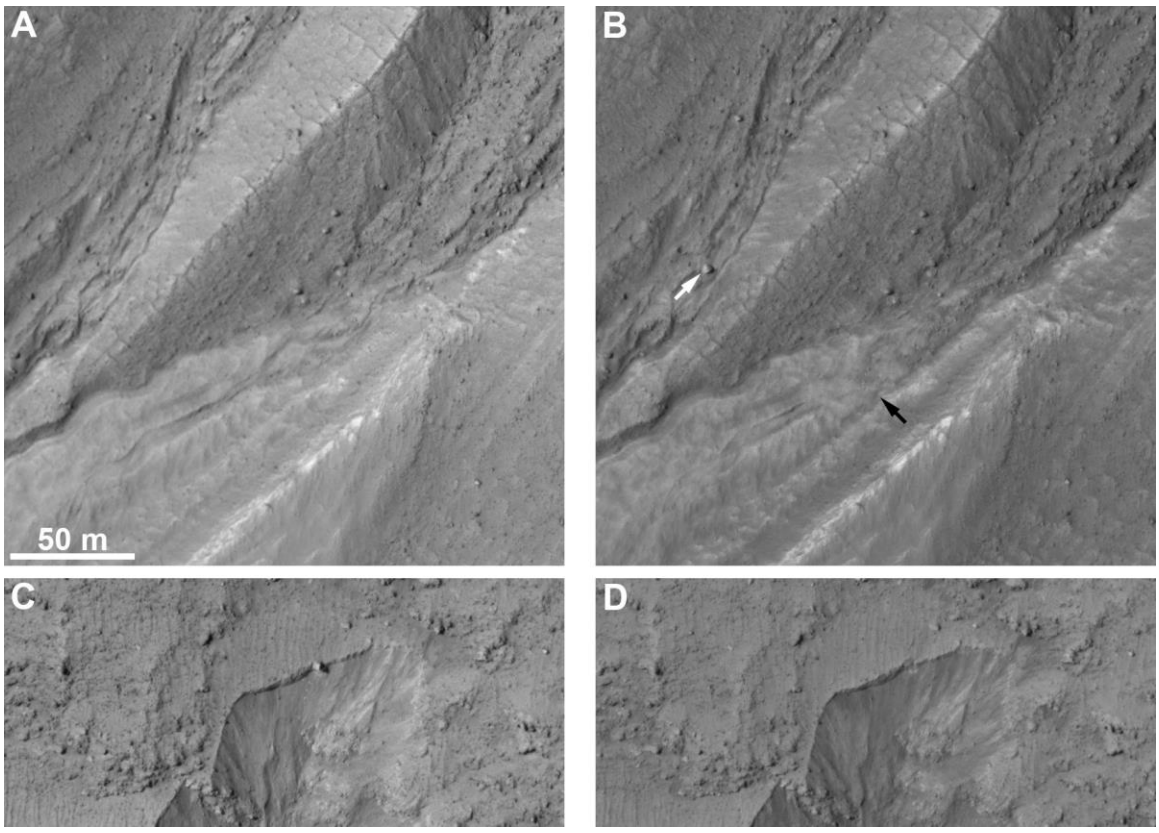

Figure 8: Flows in two adjacent gullies (37.6 ºS, 351.8 ºE). The black arrow in B shows extensive channel infill, while the white arrow shows a large boulder. C and D show the source location of the boulder, which fell due to slope retreat across a 50 m wide section of the slope crest (Animation S2). Downslope is bottom-left and north is up in all panels. (A/C: ESP_013941_1420. B/D: ESP_057839_1420.)

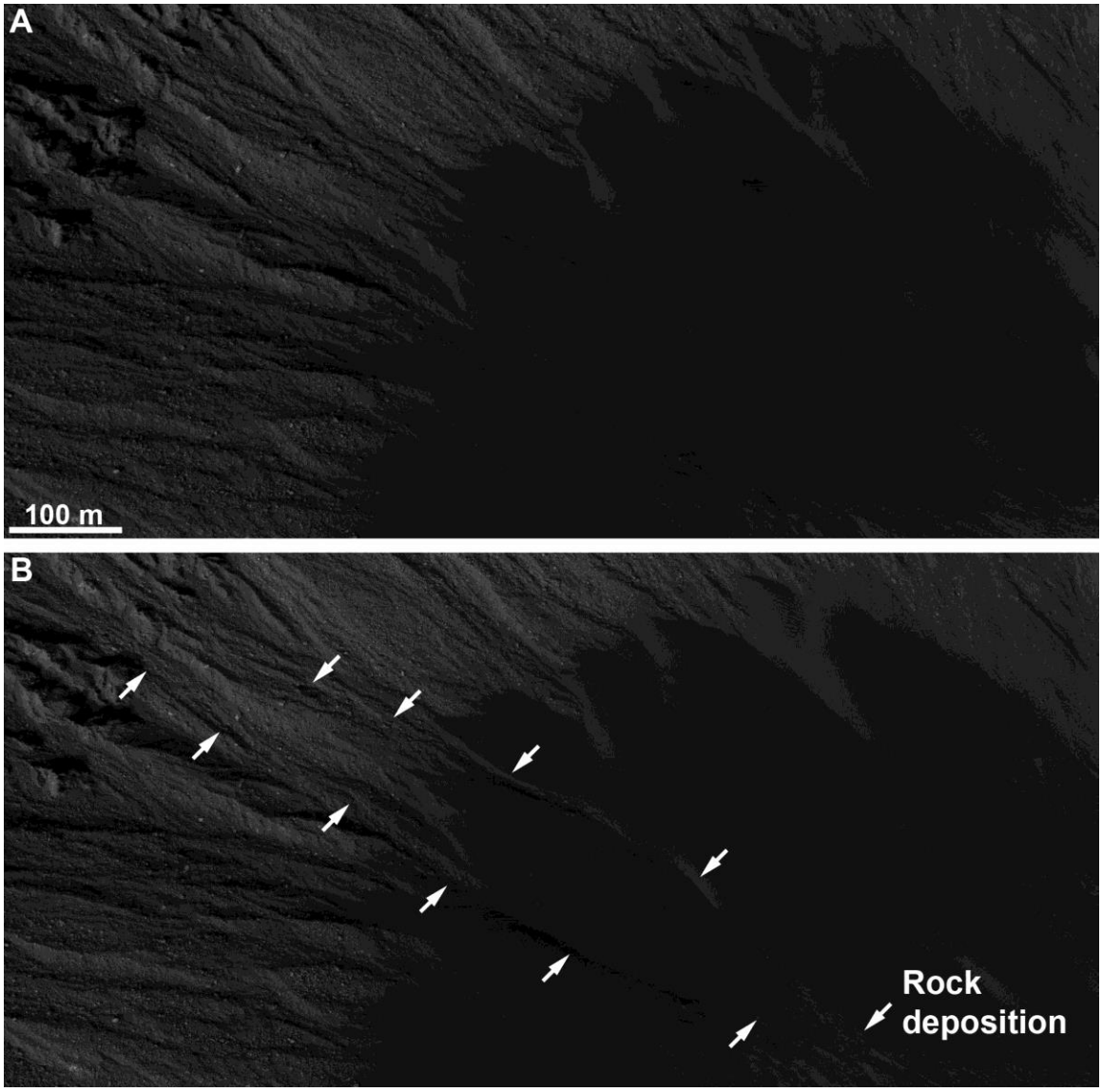

Figure 9: Large flows that began in rocky gully alcoves in Maur crater (54.6 ºN, 305.9 ºE) and transported rocky material on the upper slopes, but transitioned to eroding sand on the lower slopes. Arrows in B denote the two largest examples. Deposition occurred at lower right and continued off the edge of the figure. Although many rocks were transported on the upper slopes, little of the deposit is visibly rocky. North is up and downhill to the lower right. (A: ESP_034170_2350. B: ESP_060161_2350.)

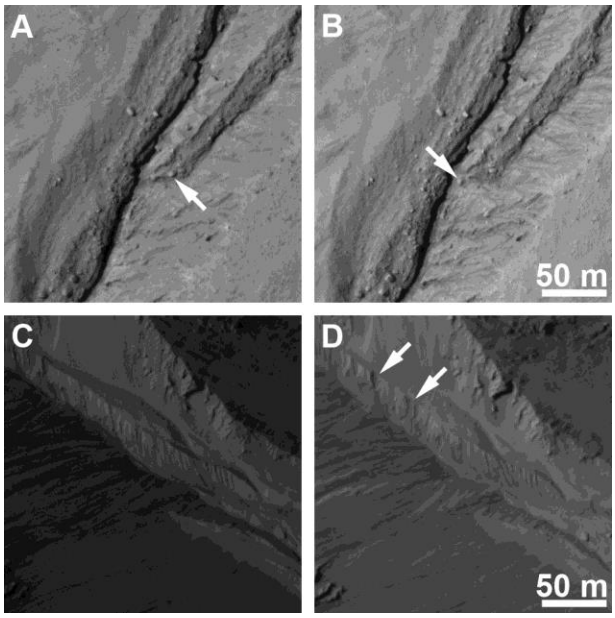

Figure 10: Examples of minor mass wasting (non-flow events) in gullies. A and B show a large rock that shifted a short distance downhill in a gully alcove (37.1 ºS, 192.1 ºE). North is up and downhill to the lower left. C and D show several minor collapses of regolith within a gully alcove in Gasa crater (35.7 ºS, 129.4 ºE). Collapses occurred at different times in spring/summer and in once case progressively grew in a three-image sequence. North is up and downhill to the lower right. (A: ESP_022808_1425. B: ESP_057924_1425. C: PSP_004060_1440. D: ESP_014081_1440.)

Supplementary Material for

"Martian Gully Activity and the Gully Sediment Transport System"

Supplementary material for this manuscript includes Tables S1–S2 (provided as separate CSV files, with a description of the fields below), Figures S1–S5 (this file, below), and Animations S1–S2 (provided as separate animated GIF files, with captions in this file). CSV files include a header row.

Table S1 has the following fields:

Field	**Explanation**
Site_ID	Identifier assigned to each site. The prefix is S or N to denote southern or northern hemisphere, followed by a unique number; one site denotes a series of overlapping High Resolution Imaging Science Experiment (HiRISE) images, and some sites are adjacent and have additional partial overlaps. A handful of site numbers have been skipped, due to inadvertent duplication or determination that the data were not useful. These numbers were not reused and other sites were not renumbered to avoid possible mistakes in the renumbering process.
Latitude	Planetocentric latitude.
Longitude	East longitude in the 0–360º system.
N_winters	Number of times the winter solstice (L_S=90º in the southern hemisphere or 270º in the north) occurs within the span of HiRISE observations for the site.
N_winters_excellent	Number of solstices where the coverage quality (lighting and geometric match) from HiRISE Reduced Data Record (RDR) images is excellent. This is a qualitative assessment.
N_winters_good	Number of solstices where the coverage quality (lighting and geometric match) from HiRISE RDR images is good. This is a qualitative assessment.
N_winters_poor	Number of solstices where the coverage quality (lighting and geometric match) from HiRISE RDR images is poor. This is a qualitative assessment and mostly indicates frost cover or major issues with shadows.
Is_active	Whether or not the site is known to be active. Field may be "y" (yes) or "n" (no). Sites classified as "n" includes those with possible/probable unconfirmed activity.
Is_active_HiRISE	Whether or not the site is known to be active with before-and-after HiRISE image coverage. Field may be "y" (yes) or "n" (no). Sites classified as "n" includes those with possible/probable unconfirmed activity.
N_flows	Number of flows observed at active sites. For site S0056, the value is given as 0 despite known activity because of challenges accurately counting the small flows which are only visible in deep shadow.

N_large_gullies	Approximate number of large gullies (those with alcoves that are substantially wider and deeper than the rest of the gully system). Only provided for 100 sites; "x" if not tabulated.
N_small_gullies	Approximate number of small gullies (those with alcoves that are not much wider and deeper than the rest of the gully system). If the value ends in 0.5 rather than an integer, the site has a significant amount of gullied slope that could not meaningfully be defined as individual gullies. Only provided for 100 sites; "x" if not tabulated.

Table S2 has the following fields:

Field	**Explanation**
Site_ID	Monitoring site ID from Table S1.
Flow_ID	Unique identifier for the change. These are constructed as follows: [S/N]xxxx_MYyy_zz. [S/N]xxxx is the site ID with the number always rendered with four digits. MYyy is the Mars year of the first image after the flow event; in many but not all cases this is the Mars year that the flow occurred. zz is a unique two-digit number to denote individual events at sites where more than one flow occurred in a given year, and is replaced with "X" for changes that were not categorized as flows (see below). For example, "S0001_MY29_01" is a flow event from Gasa crater (southern hemisphere site 1) with the first "after" image dating from Mars Year 29, and was the first flow noted for that site from that year. The Mars Year calendar is enumerated in Piqueux et al. (2015).
Site_Latitude	Planetocentric latitude.
Site_Longitude	East longitude in the 0–360º system.
Morphology	General classification of gully morphology. Includes "ACA" (alcove-channel-apron gully), "Channels" (minimal alcove or apron), "Poorly defined", and "Non-gully".
Alcove_material	Material removed to create the alcove. Includes "Rock", "Mixed", "Mantle", "Sand", "Other", or "N" (for no alcove). See main text for definitions.
Incised_material	Material eroded by the channel. Includes "Mixed", "Sand", "Other", and "N" (for no such material). See main text for definitions.
Apron_material	Material on the apron surface. Includes "Mixed", "Sand", "Other", and "N" (for no apron). See main text for definitions.
Change_material	Material of the new flow deposit. Includes "Mixed", "Sand", and "Other". See main text for definitions.
Before_image	Image ID for a HiRISE image before the flow event that can be compared to the reference image (next item). This is not necessarily the image that provides the date constraint but rather a good-quality comparison for observing the change. In some cases many comparisons are possible and better comparisons may exist. Users should note that the comparison quality is variable and careful registration and comparison may be needed to see subtler changes. "x" for flows that are visible only in shadow or over frost.

Reference_image	Image ID for a HiRISE image from after the change that shows the new feature. In most but not all cases this is the first high-quality image after the event.
X	Approximate X pixel coordinate of a distinctive feature of the change in the reference HiRISE RDR image. Increases to the right. XY coordinate (0,0) is at the upper left pixel of the image.
Y	Approximate Y coordinate of a distinctive feature of the change in the reference HiRISE RDR image. Increases downwards. XY coordinate (0,0) is at the upper left pixel of the image.
Orientation	Approximate local downhill orientation of the gullied slope. Includes "N", "NE", "E", "SE", "S", "SW", "W", and "NW".
MY_before	Mars Year of the last image before the change. (For this and the next three fields, these refer to definitive before/after images; intervening images may exist but be of insufficient quality to effectively constrain the flow timing.)
Ls_before	Areocentric longitude of the Sun (L_S), a measure of Mars season, of the last image before the change.
MY_after	Mars Year of the first image after the change.
Ls_after	L_S of the first image after the change.
Classification	Classification of the change. Includes "MajorFlow", "Flow", "ThinFlow", "Halo", and "Other". See main text for definitions. "Halo" and "Other" were not treated as flows in the analysis.
Is_bright	Whether the change is brighter than the surrounding material; "Y" or "N".
Is_dark	Whether the change is darker than the surrounding material; "Y" or "N".
Color	Relative color of the change in enhanced-color HiRISE "IRB" (Infrared, Red, and Blue-Green) images with infrared data assigned to the red channel, red data assigned to the green channel, and blue-green data assigned to the blue channel. Includes "Blue", "Yellow", "Green", "Pale", "N" (neutral color relative to surroundings), and "U" (no color data cover the change).
Is_shadow_only	Whether the flow was only visible while in deep shadow; "Y" or "N".
Channel_change	Whether there were topographic changes observed in the channel; "Y", "N", "L" (likely), or "U" (uncertain). The latter two were treated as N for analysis.
Channel_incision	Whether there was any clear evidence of erosion within the channel or extension of the channel; "Y", "N", "L" (likely), or "U" (uncertain). The latter two were treated as N for analysis.
Large_gully	Whether or not the gully was well-developed (alcove substantially wider and deeper than the rest of the system); "Y" or "N".
Reach_end	Whether or not the event flowed to the end of the channel system; "Y" or "N".
Boulder_transport	Whether or not movement of boulders was observed as part of the event; "Y" or "N".

Largest_buried	Diameter of the largest buried boulder on the apron or near the end of the channel, in meters; 0 if none.
Largest_transported	Diameter of the largest boulder moved by the event, in meters; 0 if none.
Comments	Text field with brief description of any notable features of the event; “x” if none.

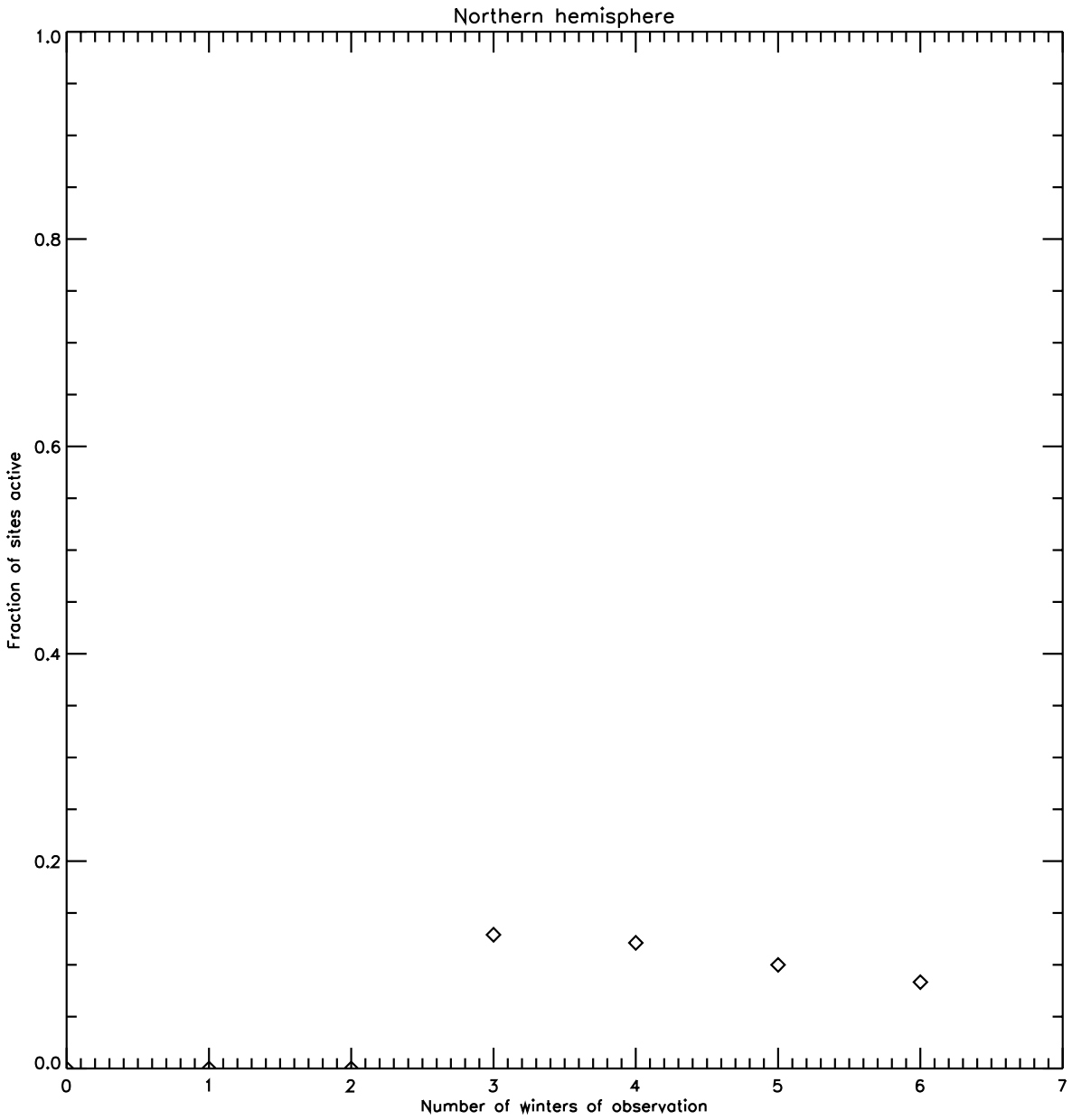

Figure S1: Fraction of gullies with observed activity as a function of the number of winter solstices spanned by monitoring images, for the northern hemisphere.

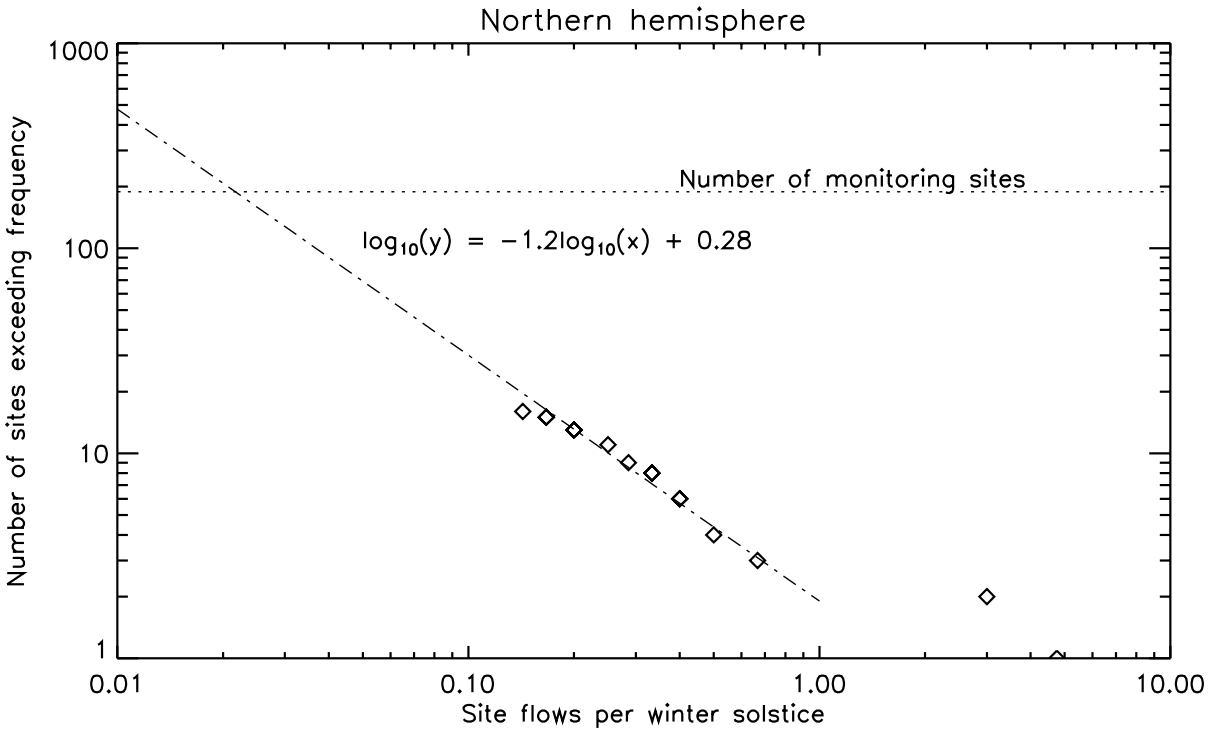

Figure S2: Cumulative plot of the number of gully sites with observed flow frequencies exceeding a given frequency, for the northern hemisphere. Power-law fit is by eye and the extrapolation to lower frequencies may be inaccurate.

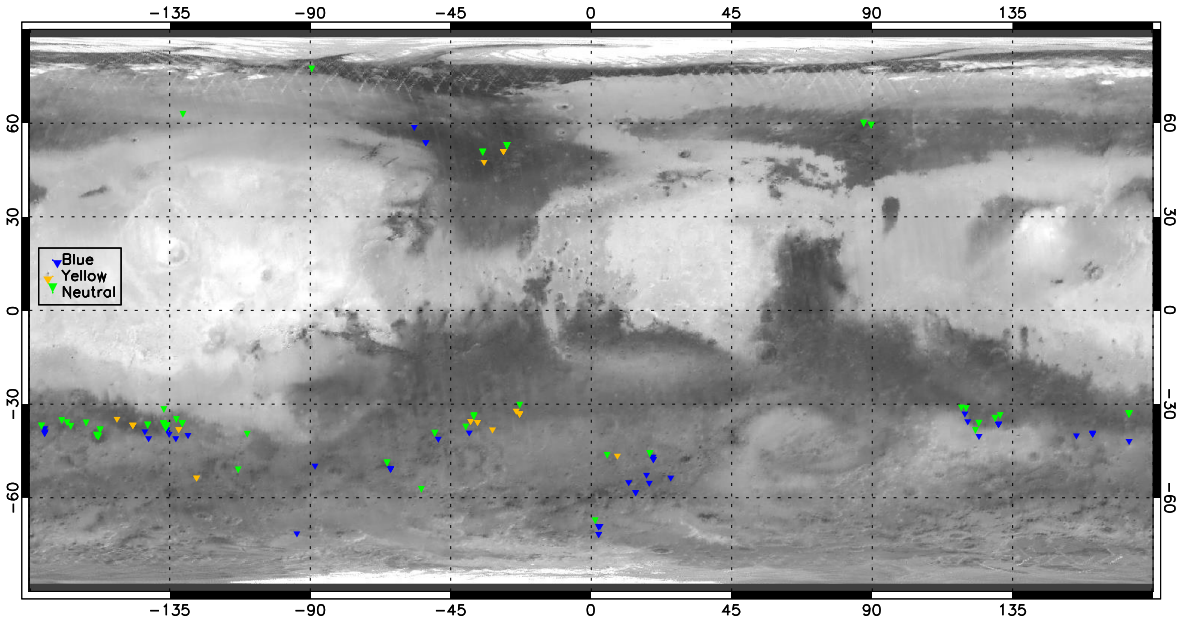

Figure S3: Map of the distribution of relative colors of gully flows ("Color" in Table S2) in HiRISE IRB images: blue, yellow, or neutral. (Green and pale flows are excluded as they are rare.) Triangles of different colors have different offsets relative to plot point to avoid overplotting of nearby points and the offset is shown in the legend. Background is albedo from the Thermal Emission Spectrometer (TES).

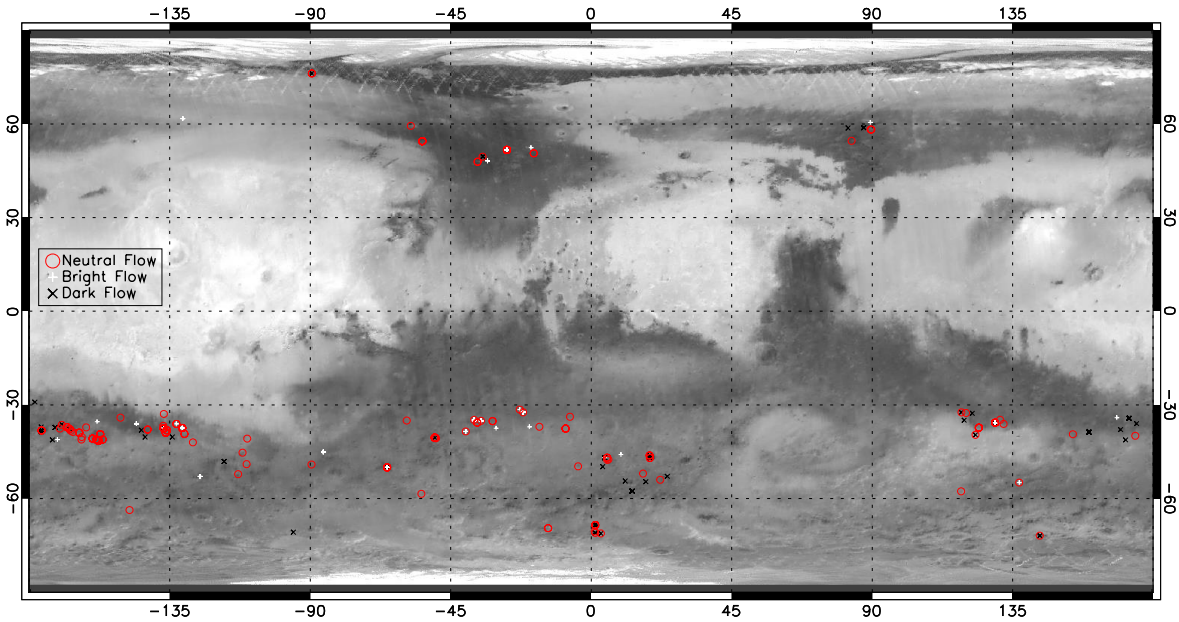

Figure S4: Map of the distribution of relative tones of gully flows: bright, dark, or neutral relative to surroundings (based on "Is_bright" and "Is_dark" in Table S2). Background is albedo from the Thermal Emission Spectrometer (TES).

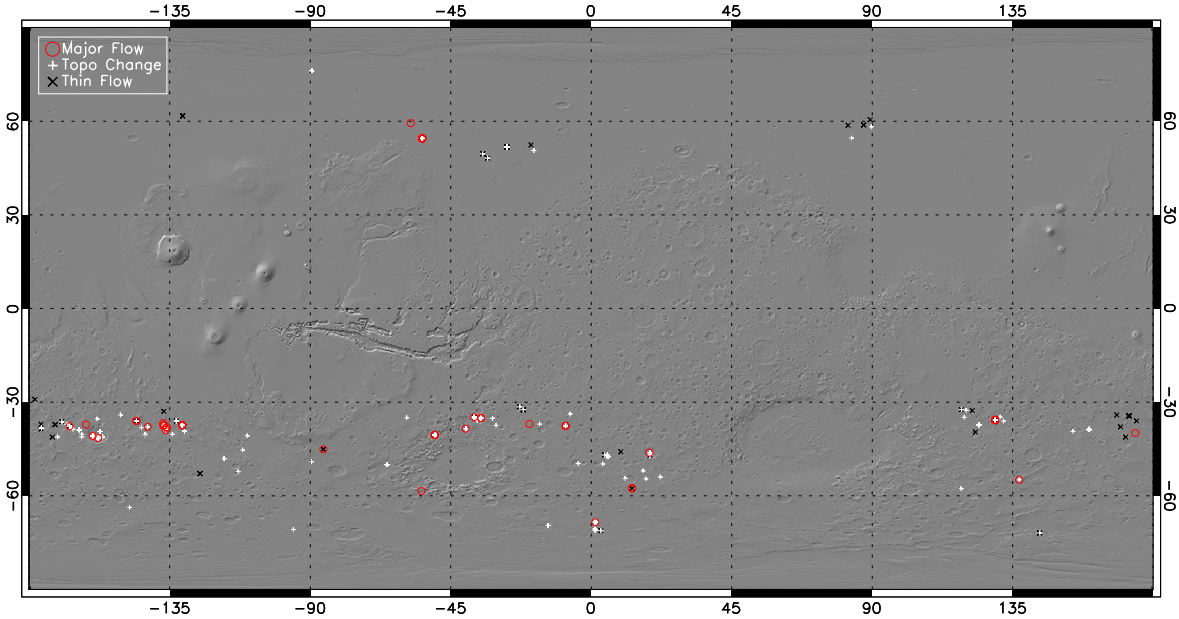

Figure S5: Map of the distribution of gully flow types: major flow, topographic changes (topo change), or thin flows ("MajorFlow", "Flow", and "ThinFlow" in Table S2). Other events are excluded. Background is shaded relief from the Mars Orbiter Laser Altimeter (MOLA) global Digital Elevation Model.

Animation S1: Blink comparison of panels A and B from Fig. 2 in the main text, showing new gully channels and deposits.

Animation S2: Blink comparison of panels C and D from Fig. 8 in the main text, showing general slope retreat in addition to the displaced boulder.